AD-A040 697 MASSACHUSETTS INST OF TECH CAMBRIDGE DEPT OF OCEAN E--ETC F/G 8/3
THE RESOLUTION OF DIRECTIONAL WAVE SPECTRA USING THE MAXIMUM LI--ETC(U)
MAY 77 O H OAKLEY, J B LOZOW N00014-76-C-0338
UNCLASSIFIED OE-77-1 NL

1 OF 1
AD A040697

END

DATE FILMED
7-77

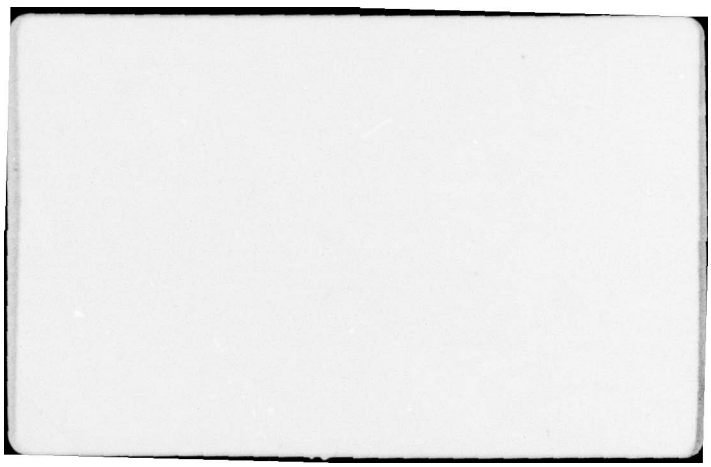

Report 77-1

THE RESOLUTION OF DIRECTIONAL WAVE SPECTRA USING THE MAXIMUM LIKELIHOOD METHOD

by

O. H. Oakley, Jr.*

J. B. Lozow*

This research was carried out under the Naval Sea Systems Command
General Hydromechanics Research Program administered
by the
Naval Ship Research and Development Center.
Contract Number N00014-76-C-0338

* Department of Ocean Engineering
Massachusetts Institute of Technology
77 Massachusetts Avenue
Cambridge, Massachusetts 02139

SECURITY CLASSIFICATION OF THIS PAGE (When Data Entered)

REPORT DOCUMENTATION PAGE

READ INSTRUCTIONS BEFORE COMPLETING FORM

1. REPORT NUMBER (14) Ocean Engineering Report 77-1
2. GOVT ACCESSION NO.
3. RECIPIENT'S CATALOG NUMBER

(6) 4. TITLE (and Subtitle)
The Resolution of Directional Wave Spectra Using the Maximum Likelihood Method,

5. TYPE OF REPORT & PERIOD COVERED
Final - 1 Oct. 1975 - 31 Dec. 1976

6. PERFORMING ORG. REPORT NUMBER

(10) 7. AUTHOR(s)
O. H. Oakley, Jr.
J. B. Lozow

(15) 8. CONTRACT OR GRANT NUMBER(s)
N00014-76-C-0338 new

9. PERFORMING ORGANIZATION NAME AND ADDRESS
Department of Ocean Engineering
Massachusetts Institute of Technology
Cambridge, Massachusetts 02139

10. PROGRAM ELEMENT, PROJECT, TASK AREA & WORK UNIT NUMBERS
(12) 87 p.

11. CONTROLLING OFFICE NAME AND ADDRESS
David W. Taylor Naval Ship R & D Center
Bethesda, Maryland 20084 (Code 1505)

(11) 12. REPORT DATE
May 1977

13. NUMBER OF PAGES
vii + 78

14. MONITORING AGENCY NAME & ADDRESS (if different from Controlling Office)
Office of Naval Research
Resident Representative, MIT, Room E19-628
Cambridge, Massachusetts 02139

15. SECURITY CLASS. (of this report)
Unclassified

15a. DECLASSIFICATION/DOWNGRADING SCHEDULE

16. DISTRIBUTION STATEMENT (of this Report)

Approved for public release; distribution unlimited.

(9) Final rept. 1 Oct 75 - 31 Dec 76,

17. DISTRIBUTION STATEMENT (of the abstract entered in Block 20, if different from Report)

Summary presented at the Offshore Technology Conference Houston, Texas, May 1977. Paper No. OTC 2745.

18. SUPPLEMENTARY NOTES

Sponsored by the Naval Sea Systems Command, General Hydromechanics Research Program administered by David W. Taylor Naval Ship Research and Development Center, Code 1505, Bethesda, Maryland 20084.

19. KEY WORDS (Continue on reverse side if necessary and identify by block number)

Wave Spectra (Directional)

Maximum Likelihood Method (MLM)

20. ABSTRACT (Continue on reverse side if necessary and identify by block number)

The Maximum Likelihood Method is examined for use in measuring the directionality of ocean wave spectra in conjunction with sparse wave-gage arrays. Directional characteristics of small wave-gage arrays and the effects of noise, wavelength, and gage spacing are analyzed via simulated input spectra. A figure of merit is derived as an aid in array design.

DD FORM 1 JAN 73 1473 EDITION OF 1 NOV 65 IS OBSOLETE
S/N 0102-014-6601

SECURITY CLASSIFICATION OF THIS PAGE (When Data Entered)

406 856

mt

ABSTRACT

The Maximum Likelihood Method is examined for use in measuring the directionality of ocean wave spectra in conjunction with sparse wave-gage arrays. Directional characteristics of small wave-gage arrays and the effects of noise, wavelength, and gage spacing are analyzed via simulated input spectra. A figure of merit is derived as an aid in array design.

TABLE OF CONTENTS

FIGURES

NOMENCLATURE

a_n - nth complex coefficient in Fourier series expansion of $F(\theta)$

A - wave amplitude

$A_i(\omega;T)$ - Fourier transform of $\eta_i(t)$

$B[\theta;\omega|\theta_o;\omega_o]$ - beam pattern

$C(\omega,\underline{r})$, C_{ij} - covariance matrix (spatial), matrix elements

$E\{\ \}$ - expected value operator (statistical average)

$E_m(\theta)$ - equivalent to $\exp[j\ \underline{k}\cdot\underline{r}_m]$

$F(\theta)$ - normalized directional spectrum spreading function

f - frequency in cycles/second

F.O.M. - figure of merit

H - wave height (twice wave amplitude)

$J_k(\ )$ - kth order Bessel function

$\underline{k}$, $k(\omega)$ - wavenumber (vector), wavenumber (scalar)

$n(\underline{x},t)$ - noise signal

N - number of array elements or sensors

$N(\omega)$ - noise power level in frequency domain

$P(\theta_o;\omega_o)$ - weighted measure of array performance

$\overline{P}(\omega_o)$ - average of $P(\theta_o;\omega_o)$ over all θ_o angles

$\overline{Q}'$ - figure of merit, F.O.M.

$Q_{ij}(\omega)$ - element of the inverse of covariance matrix [ij(ω)]

$\underline{r}_i$ - radius vector to array elements i

$\underline{r}_{ij}$ - gage pair position vector

$S(\omega)$, $S_{ij}(\omega)$ - point spectrum, cross spectra

T	- length of time record
$W_i(\theta_o;\omega_o)$	- weighting coefficients associated with beam pattern
$W(t)$	- taper function in time domain
$W(\omega)$	- Fourier transform of W(t) (window function)
x,y	- coordinates in physical space
x_c	- position vector of ith sensor
Δp	- pin spacing width on pin type wave detector
$\eta_i(t)$	- time history associated with ith wave sensor
θ	- azimuthal angle coordinate associated with $\underline{k}$
λ	- wavelength
σ	- standard deviation
ϕ_{ij}	- argument of sensor pair (i,j) vector
ω	- frequency in radians/second

Superscripts

$\hat{}$	- denotes a measured quantity
$*$	- denotes complex conjugate
N	- denotes total normalized elements in array

I. INTRODUCTION

Oceanographic literature of the past twenty years provides a wealth of descriptions and techniques for the mathematical modeling of ocean waves. Since the acceptance of stochastic processes as a viable tool for the behavioral prediction of surface waves, considerable effort has been expended in an attempt to measure and predict the structure of the wave spectrum associated with given wind speeds. The spectral description for time histories describing the surface elevation at an arbitrary point are fairly well developed and are widely used, although the parameterized model in vogue changes rapidly (cf Hasselman, 1973 and 1976; Pierson, 1976). However, the issue as to how the spectrum is distributed over direction is by no means well understood. Current knowledge of the angular spreading of wave spectra is minimal and wave forecasting awaits a sufficient data base upon which to build satisfactory directional models.

Essential to the establishment of such a data base are, obviously, spectral estimation techniques of sufficient resolution. With the advent of the Fast-Fourier-Transform (FFT) and data-adaptive spectral analysis techniques (e.g., the MLM), vast quantities of raw recorded data may be handled efficiently by computers such that temporal processes are readily digested and spectrally analyzed. Directional spectra naturally involve spatial transforms and spatial cross correlations from observations, typically over a small portion of the wave field. Relatively few observation or recording points can cause poor angular resolution of the spectral estimate. This may be observed in the following examples.

Directional wave spectra estimates were determined from measurements obtained in San Francisco Bay and extensively reported in Chou, et al, (1974). Two contour plots of wave energy density spectra $S(\omega,\theta)$ are shown in Figures I-1 and I-2 where frequency increases radially and wave direction corresponds to the angular variable. Though somewhat difficult to see in these plots, both examples suggest that there was a considerable amount of directional spreading of the wave energy. On the other hand, observers at the time were impressed by the relative narrowness of the wave

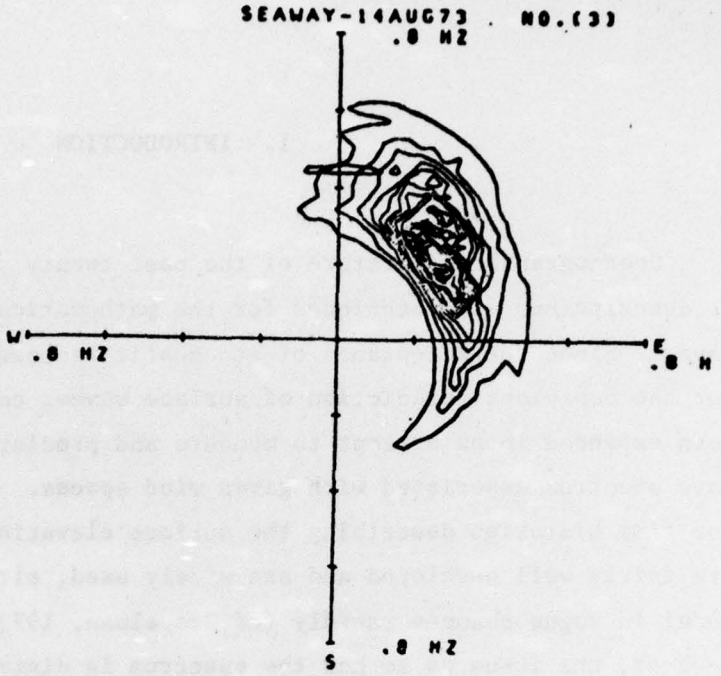

FIGURE I-1

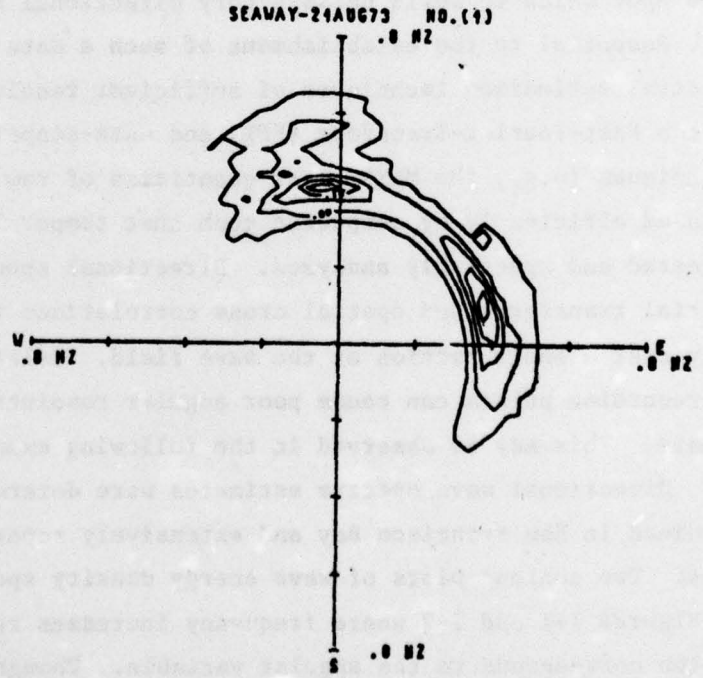

FIGURE I-2

distribution and the lack of spectral energy from direction other than the principle wind wave sources. Some of the ship motion predictions using the measured directional spectra were improved if the spectra were truncated in direction so as to include only the most energetic parts of the spreading function. Figure I-2 is a particularly dramatic example of "cross seas," two wind wave systems radiating into the measurement area at right angles. The contours connecting the two principle peaks are most likely spurious and are due to the analysis of the particularly small array of wave sensors used inthe experiments. Improved resolution can be obtained by increasing the array size, though often at considerable cost. Since the spectral analysis was done using the data adaptive Maximum Likelihood Method (MLM), an exceptionally high resolution technique, it is possible that the field observations and ship motions theory are equally to blame for the apparent lack of experimental and theoretical correlation. An analysis of the resolution potential of small arrays and the (nonlinear) MLM spectral estimation techniques appears to be in order and is the subject of this report.

Chapter II describes some of the wave measuring systems and array geometries in use. Chapter III reviews the normal recording and spectral analysis steps in array data preparation and Chapter IV discusses array resolution in terms of the beam pattern. Chapters V, VI, and VII provide the wave spectral simulation and the array sensitivity analysis.

II. MEASURING SYSTEMS

In order to determine the wave number spectrum of the sea surface, it is necessary to obtain a measure of the wave amplitude, or related variable, over a region of space. Photographic and optical reflection techniques are attractive in principle, but clumsy to work with in practice (cf. Cote, et al, 1960 and Pierson,1976). Many of these techniques are only appropriate for the short-gravity-wave and capillary-wave regions (Guthart, et al, 1975). Land and satellite based wave measuring systems at present all suffer from insufficient resolution. Only fixed spatial arrays of wave sensors are repeatedly used with success in the spatial measurement of wind generated gravity waves. For this reason, scanning techniques and the combination of fixed and scanning sensors (cf. Mollo-Christensen & Koziol, 1972) will not be considered in this report. They not only require special treatment in the interpretation of their spectral analysis due to Doppler shift effects, but they also require special consideration in the construction of the covariance matrix described in Chapter IV.

The communications and siesmic literature is replete with analyses and optimum design procedures for large arrays, i.e., arrays that could contain from tens to hundreds of elements (Capon, 1969). However, water wave arrays have not exceeded six elements, with three and four sensors being the most common. These arrays are extremely small and certainly do not permit approximate design procedures based on a continuous distribution of elements. A typical array configuration is shown in Figure II-1 along with the wave heading angle definition.

The most common wave sensors are wave staffs, bottom mounted pressure transducers, and tethered buoys. The wave staffs use the sea water as an electrical short circuit and are either of the resistive or capacitive type. The former allows the sea water to modulate the resistance of a bare wire or short-out successive pins (step type). The latter is designed to measure the capacitance between a dielectrically clad wire and the water. Pressure transducers are attractive because, unlike the wave

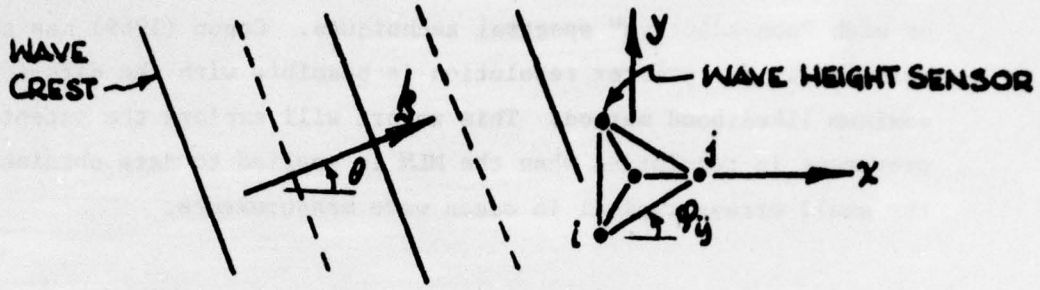

Fig. II-1 Definition Sketch: Array Pattern with four elements

staffs, they do not require a special (possibly reflecting) structure on which to mount them and are relatively safe from the standpoint of vessel operations. On the other hand, they are more difficult to locate precisely and have poor high frequency response. Tethered buoys have advantages in deep water since they can be placed where a fixed structure would not be practical. However, extracting the wave time history from the buoy motions and establishing the relative position of the members of the buoy array are likely to be difficult tasks at best. There are a large number of review papers describing wave measuring and monitoring systems. Relatively current bibliographies can be found in Pierson (1976), Guthart, et al (1976), and Panicker (1974). A list of regularly used wave measuring devices is given by Draper and Fortnum (1974).

Numerous array geometries have been used and it is appropriate to cite a few of the larger and more recent examples. Bennett (1964) employed a six-gage array of pressure gages in the Gulf of Mexico. A five-gage array was installed by the Corps of Engineers off the California coast (Borgman and Panicker, 1970) and the configuration is shown in Figure A-1 (f) of Appendix A. More recently, a four-gage array of wave staffs was used in San Francisco Bay (Haddara, et al, 1972) and the resulting directional spectra reported by Chou, et al (1974). Deep Oil Technology recently completed their large scale Sea Test Program of a Tension Leg Platform off of Catalina Island, California. A six-gage array of wave staffs, similar to the one sketched in Figure A-1(e), was used and the data reported to NOAA's Environmental Data Service (NODC, 1976). Except for the last two test programs, the analysis of the data obtained from the arrays reported to date have been analyzed only for the principle wave direction

or with "non-adaptive" spectral techniques. Capon (1969) has shown that potentially far greater resolution is possible with the data-adaptive maximum likelihood method. This report will explore the potential improvement in resolution when the MLM is applied to data obtained from the small arrays typical in ocean wave measurements.

III. SPECTRAL ANALYSIS

1. Temporal Spectral Estimation

Computational schemes for estimating the power spectral density of a stationary, random, time-varying recorded signal have been developed in the last quarter century. Initially, the basic procedure was to form an estimate of the temporal correlation function which was directly transformed to a "frequency-domain" to provide an estimate of the spectral density. This, more or less, is the methodology advanced by Blackman and Tukey (1959). In 1965, Cooley and Tukey introduced the computationally superior Fast Fourier Transform (FFT) technique to obtain spectral estimates. This method employs the product of the transformed time series rather than the conventional transform of a synthesized correlation function. Both of the above methods will be generally referred to as <u>direct</u> spectral estimators.

For example, suppose an estimate of the cross-spectrum of two measured time histories $\hat{\eta}_1(t)$, $\hat{\eta}_2(t)$ is desired and these records are each of length T. Let $A_i(\omega;T)$, the direct Fourier transform, be defined as:

$$A_i(\omega;T) = \int_{-T/2}^{T/2} \hat{\eta}_i(t) W(t) e^{-i\omega t} dt. \quad (i=1,2) \tag{3.1}$$

Here, the $\hat{\eta}_i(t)$ and $A_i(\omega;t)$ are random variables and W(t) is a suitable taper function. The (FFT) spectral estimate is then given by:

$$\hat{S}_{12}(\omega;T) = \frac{A_1(\omega;T) A_2^*(\omega;T)}{\int_{-\infty}^{\infty} |W(\omega)|^2 d\omega}. \tag{3.2}$$

This estimate has the property that:

$$\lim_{T\to\infty} E\{\hat{S}_{12}(\omega;T)\} \longrightarrow S_{12}(\omega)$$

where $S_{12}(\omega)$ is the true cross-spectrum.

Tapering is inherent to all spectral estimation procedures and is applied for numerical stability of the spectral estimate. The taper function is applied directly to the estimated autocorrelation function (Blackman-Tukey method) or the time series (FFT) method before any Fourier transforms are calculated. The shape and duration of the taper function are determined a priori through consideration and trade-offs of desired spectral resolution and statistical variance. The window function is the Fourier transform of the taper function and relates the average estimated spectrum to the true spectrum. Proper taper/window function design is difficult in that high frequency resolution tends to be achieved at the expense of statistical reliability, and for limited amounts of data, this phenomenon is particularly troublesome and statistical reliability is particularly poor. The dominant characteristic of direct or conventional algorithms is that the taper or window function is prescribed and does not depend on the true spectrum being estimated, cf. Otnes and Enochson (1972).

Within the last ten years powerful data adaptive methods have developed to alleviate the windowing problem. These methods are generally termed "nonlinear" vs. the direct or linear methods previously mentioned. The window associated with these methods depends on the true spectrum as well as the power at the particular frequency being estimated. It adapts in an optimal way so as to be least "disturbed" by noise or signal power in adjacent frequency bands. Two different nonlinear methods are currently available: 1) the maximum likelihood method (MLM) is designed to minimize the error, in a least squares sense, of the spectral estimate, and 2) the maximum entropy method (MEM) which though not yet state-of-the-art has the highest potential resolution capabilities (Lacoss, 1971). The MEM is somewhat more difficult to compute and the spectrum is not interpretable in the same way as the usual power density spectrum. It is therefore not as useful a tool for engineering analysis.

The MEM method is still being refined and is not in general use. Consequently, this study will emphasize the direct and MLM techniques.

2. Spatial Spectral Estimation

The measurement of the frequency-wave number spectrum in a multidirectional seaway by means of static arrays is done by employing the spatial analogs of the temporal estimation schemes discussed previously. The window functions are now addressed to wave number space (magnitude and direction). The directional window function is called the array beam pattern. The beam pattern associated with the direct or conventional frequency-wave number estimation is called the "natural" beam pattern. As in the pure time series analog, the natural beam pattern does not adapt to the wavenumber spectrum being estimated, but depends entirely on the geometric configuration of the array. Similarly, an "effective" beam pattern is associated with the adaptive or nonlinear methods. This directional window adjusts to minimize interference from directional components in neighborhoods adjacent to the direction of immediate interest.

The formulation of the direct and MLM spectral estimates are given as follows. Covariance matrix elements $C_{ij}(\omega)$ are defined as:

$$\hat{C}_{ij}(\omega) = \frac{1}{T} A_i(\omega;T) A_j^*(\omega;T) \tag{3.3}$$

where $A_i(\omega;T)$ is the Fourier transform of the measured wave amplitude $\hat{n}_i(t)$ as in Equation (3.1). The matrix elements are generally normalized using the deviations $\sigma_i(\omega) = \sqrt{S_{n_i}(\omega)}$ in order to reduce the effect of calibration errors, i.e.,

$$\hat{C}_{ij}^N(\omega) = \frac{\hat{C}_{ij}(\omega)}{\sigma_i(\omega)\sigma_j(\omega)} .$$

The direct frequency-wavenumber spectral estimate is given by

$$\hat{S}(\omega;\underline{k}) = \sum_{i=1}^{N}\sum_{j=1}^{N} \hat{C}_{ij}(\omega) e^{-i\underline{k}(\omega)\cdot\underline{r}_{ij}} \tag{3.4}$$

whereas the maximum likelihood estimate of the spectrum is (Capon, 1969):

$$\hat{S}(\omega,\underline{k}) = \left[\sum_{i=1}^{N}\sum_{j=1}^{N} \hat{Q}_{ij}(\omega)\, e^{-j\underline{k}(\omega)\cdot\underline{r}_{ij}}\right]^{-1} \qquad (3.5)$$

where $\hat{Q}_{ij}(\omega)$ are elements of the inverse of the matrix $\|\hat{C}_{ij}(\omega)\|$.

For our purposes it is assumed that the covariance elements $\hat{C}_{ij}(\omega)$ are reliable estimates since, in practice, T, the record length, is typically large.

3. Recording and Analysis Procedure

The measurement and analysis procedure typically employed for wave studies is shown in Figure III-1. Such a format is implicit in the simulation and analysis steps discussed below. Detailed considerations in the measurement and temporal spectrum analysis steps are given by Bendat and Piersol (1971). The problem of spectral estimate variance reduction, often called smoothing, is discussed by Jenkins and Watts (1969) and Otnes and Enochson (1972).

It is assumed that the requirements for good, normalized estimates of the covariance matrix $\|\hat{C}_{ij}^{N}(\omega_n)\|$ can be met. The remainder of this report will address the problem of directional spectrum resolution, particularly for the MLM applied to array analysis.

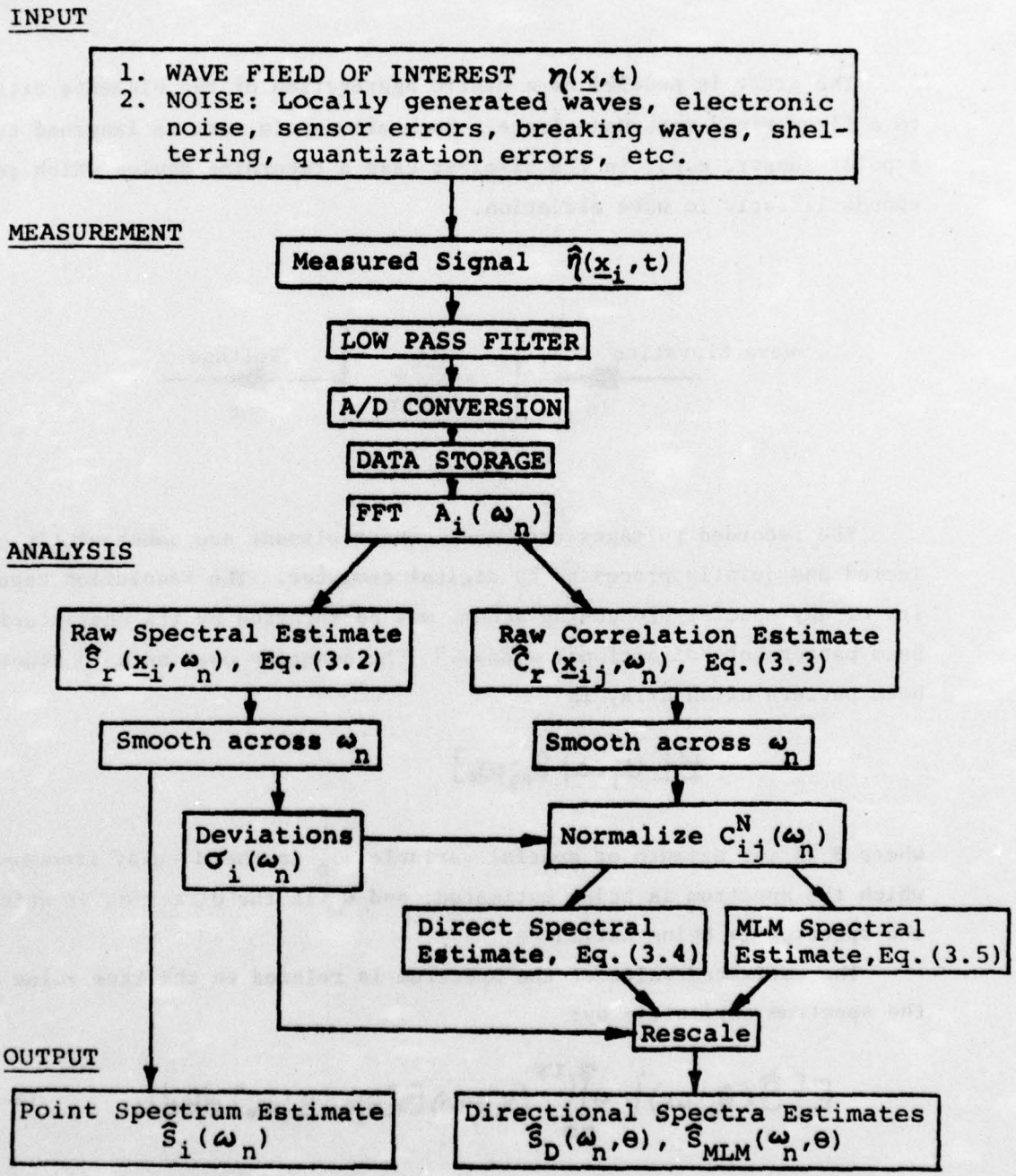

FIGURE III-1 Recording and Analysis Procedure

IV. MATHEMATICAL DESCRIPTION OF THE BEAM PATTERN

The array is modeled as a static aggregation of the elements attached to a fixed rigid reference frame. Each element in turn is imagined to be a point sensor, e.g., in the simplest case a recording device which responds linearly to wave elevation.

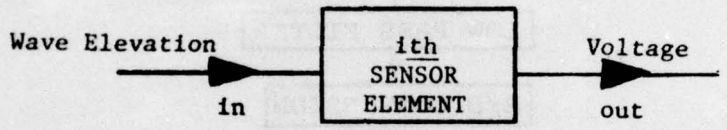

FIGURE IV-1

The recorded voltages from each sensor element are subsequently collected and jointly processed by digital computer. The resolution capability of any spatial processing scheme may be inferred by its characteristic beam pattern or "directional window." The quantity used here to denote the beam pattern of an array is

$$B[\theta;\omega|\theta_o;\omega_o]$$

where θ is the azimuth or spatial variable; ω_o is the circular frequency at which the spectrum is being estimated; and θ_o is the direction at which the spectrum is being estimated.

The estimated value of the spectrum is related to the true value of the spectrum explicitly by:

$$E\{\hat{S}(\theta_o;\omega_o)\} = \int_0^{\infty}\int_0^{2\pi} S(\theta,\omega)B[\theta;\omega|\theta_o;\omega_o]\,d\theta\,d\omega \qquad (4.1)$$

where $S(\theta,\omega)$ is the true frequency-wavenumber spectrum, $S(\theta_o,\omega_o)$ is its estimate at $(\theta_o\omega_o)$, and $E\{\ \}$ denotes the expected value operator. Roughly speaking, the most desirable beam pattern is that which is "smooth" about the estimation point $(\theta_o\omega_o)$ and negligible elsewhere, i.e., in the limit a vanishingly small slit centered about the estimation point. As indicated by Expression (4.1), the true spectrum is "leaking" through the spatial window offered by the beam pattern in yielding an estimate of $S(\theta_o\omega_o)$. The exact structure of the beam pattern depends entirely on the spatial configuration of the array and the nature of the processing involved.

In general, a (discrete array) beam pattern may be written as,

$$B[\theta;\omega|\theta_o;\omega_o] = \sum_{i=1}^{N}\sum_{j=1}^{N} W_i(\theta_o;\omega_o)W_j^*(\theta_o;\omega_o)e^{j\underline{k}(\omega)\cdot\underline{r}_{ij}} \tag{4.2}$$

where N = number of sensor elements

$\underline{r}_{ij} = \underline{x}_j - \underline{x}_i$ = gage pair position vector

$\underline{k}(\omega)$ = the wavenumber vector

$W_i(\theta_o;\omega_o)$ = weighting coefficients, in general modified for each estimation point (θ_o, ω_o).

It is customary to define the weights $W_i(\theta_o, \omega_o)$ so that:

$$B[\theta_o;\omega_o|\theta_o;\omega_o] = 1. \tag{4.3}$$

The simplest form of (4.2) is the so-called "natural" beam pattern. In this case,

$$W_i(\theta_o;\omega_o) = \frac{1}{N}e^{j\underline{k}(\omega)\cdot\underline{x}_i} \tag{4.4}$$

where $\underline{k}_o(\omega) = k_o[\cos\theta_o, \sin\theta_o]$ and k_o is obtained from the dispersion relation $\omega^2 = gk_o\tanh k_o h$. The natural beam pattern becomes:

$$B[\theta;\omega|\theta_o;\omega_o] = \frac{1}{N^2}\sum_{i=1}^{N}\sum_{j=1}^{N} e^{j(\underset{\sim}{k}-\underset{\sim}{k}_o)\cdot\underset{\sim}{r}_{ij}}. \qquad (4.5)$$

Thus, the natural beam pattern's characteristics are determined entirely by the location and number of its sensors, $\{\underset{\sim}{x}_i\}, i=1,\ldots,N$. A typical example is an array of two concentric triangles shown in Figure IV-2.

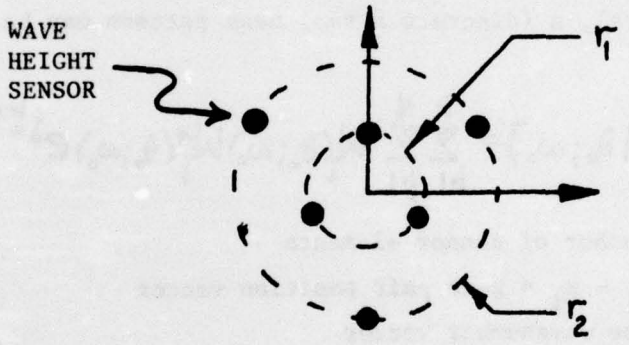

Figure IV-2

The array is more or less symmetric with rings of three elements each at radii r_1, r_2 respectively. The natural beam pattern with ω held fixed is given approximately by:

$$B_N[\theta;\omega|\theta_o;\omega_o] \cong \frac{1}{4}\left(J_o\left(2r_1 k \sin\left(\frac{\theta-\theta_o}{2}\right)\right) + J_o\left(2r_2 k \sin\left(\frac{\theta-\theta_o}{2}\right)\right)\right)^2 \qquad (4.6)$$

where $J_o(\ )$ is the 0^{th} order Bessel functions and $\omega^2 = gk \tanh kh$. This expression, containing the lead terms describing the structure of the array, exhibits the typical characteristics of sparse arrays. In particular, as $r_1, r_2 \to \infty$, the main beam narrows in the neighborhood of $\theta=\theta_o$, which is desirable. In fact, it may be shown that the "half power" beamwidth of the major lobe of the natural pattern of any array is given by:

$$(\Delta\theta)_{1/2} = \frac{360}{\pi k}\left(\frac{1}{N}\sum_{i=1}^{N}|\underline{x}_i|^2\right)^{-1/2} \qquad (4.7)$$

Note that Eq. (4.7) implies that the beamwidth is inversely proportional to the root-mean-square distance of the sensor elements from the center of the array. However, as the RMS distance becomes larger, sidelobe levels become more significant which in turn degrades the array performance through leakage. (This is not evident in Expression (4.6), however, as the secondary lobe structure has been suppressed for compactness). The natural beam pattern is inherent to the straightforward direct spectral estimation techniques and the design problem is the trade-off between beamwidth and sidelobe level.

A concise, introductory treatment of the (natural) resolution capabilities of static arrays was presented by Barber (1961) some years ago (a synopsis of which was included in the work of Barnett, 1969). Some simple arrays that are examined in order to assess their resolving power are the line array, the triangular array, and the star array. As nonlinear spectral estimation methods were not known at the time, the underlying framework of the discussion appeals to direct methods of spectral estimation. The two figures shown in Figure IV-3 are reproduced from Barber (1961). They represent contour plots of the beam patterns for a triangular and a four-element array respectively. The coordinate space corresponds to wavenumber space ($\underline{k}$ - space).

The arrays are "steered" to a particular wavenumber $\underline{k}_o=[l_o,m_o]$ The directional aspects of the array(s) may be ascertained from the intersection of the locus of points on the circle of radius $|k|=k_o$ with the contours of the beam pattern as suggested in Figure IV-3(e). A more detailed discussion is given by Barber.

For the more sophisticated adaptive techniques, the natural beam pattern does not apply. One must instead introduce the effective beam pattern. The MLM technique in particular weights the information from each sensor in an optimal manner depending upon the statistics

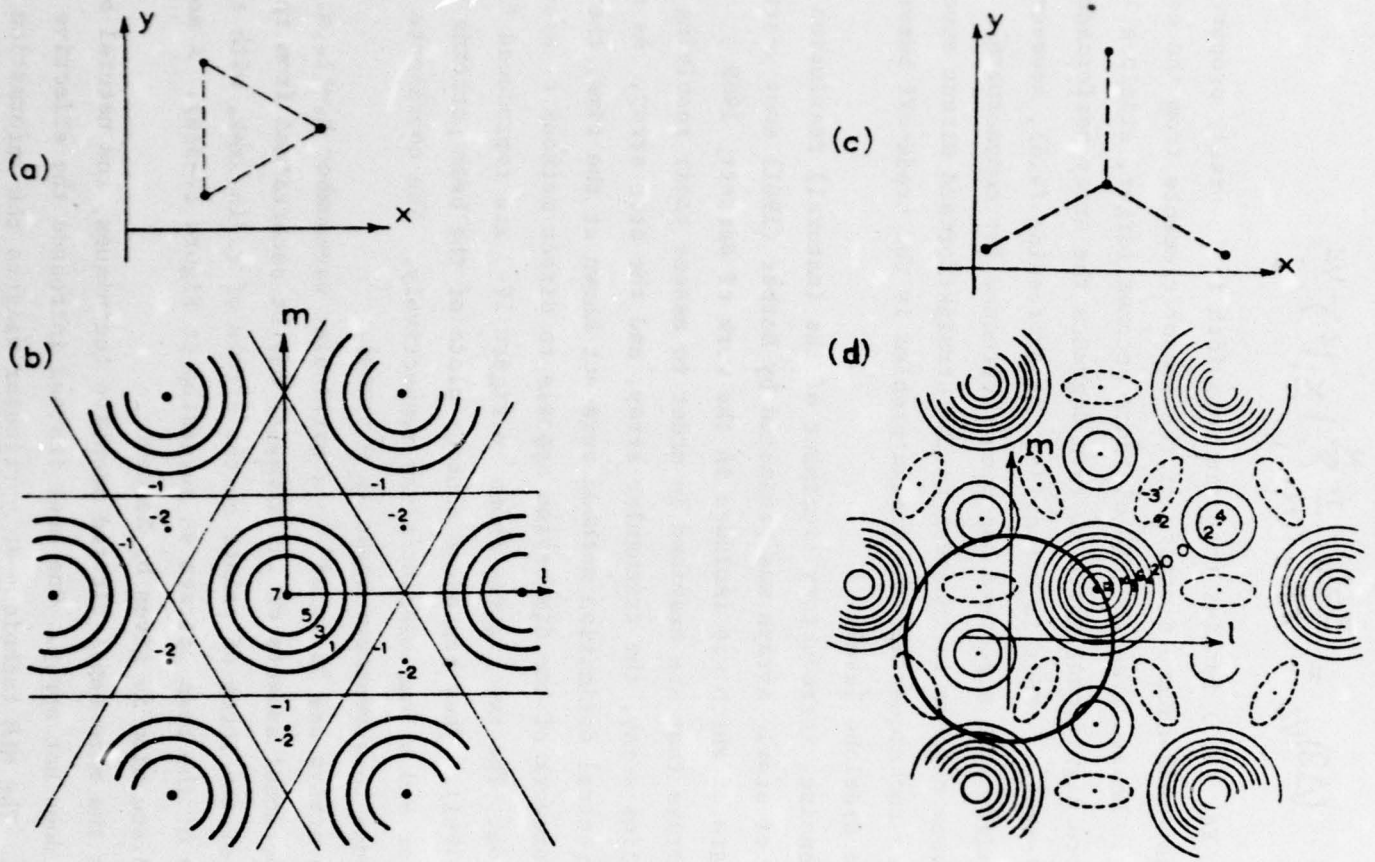

(a) Beam Pattern for a Triangular Array

(b) Calculation of the Beam Pattern for a Single Wave Train Using a Four-Element Array

FIGURE IV-3 Natural Beam Patterns from Barber (1961)

of the wave field itself (i.e., "adaptive"). The effective beam pattern for the maximum likelihood method may be written in the form:

$$B_{MLM}[\theta;\omega|\theta;\omega_o] = \sum_{i=1}^{N}\sum_{j=1}^{N} W_{ij}(\theta;\omega|\theta_o;\omega_o)\, e^{j(\underline{k}-\underline{k}_o)\cdot\underline{r}_{ij}} \quad . \tag{4.8}$$

A comparison of Eqs. (4.5) and (4.8) reveals the additional weighting coefficients $W_{ij}(\theta;\omega|\theta_o;\omega_o)$ in the latter. As the functional notation implies, these coefficients vary for <u>each</u> choice of (θ_o, ω_o), and are unique for a given array geometry, sensor noise and wave field. The result is that the MLM method (as well as other adaptive schemes) can potentially resolve a wave spectrum with greater overall precision than the traditional direct spectral analysis techniques which rely, in effect, on the natural beam pattern of the array.

The effectiveness of these data adaptive techniques can be demonstrated by simply plotting representative beam patterns generated for a particular wave field. Consider, for simplicity, a directional spectrum of the form:

$$S(\omega,\theta) = S(\omega)\, F(\theta)$$

where $F(\theta)$ is the "normalized directional spectrum spreading function," and the three element array pictured in Appendix A, Figure A-1(a). The signals received at each sensor of the array will be assumed to be noise free, i.e., there is no additional energy or ambiguity associated with the time series to be processed. This is never true in practice, cf. Chapter IV, but the resulting beam patterns are a particularly dramatic example of the power of adaptive techniques.

Let us now consider what properties we would wish the beam pattern of an array to possess. Since the true spectrum is multiplied by the beam, and integrated over direction, we would like the beam to be unity in the direction of interest, say θ_o, and suppressive at any other direction. This, of course, would be accomplished if the pattern was zero everywhere but the direction of interest, i.e., the "look" or target angle. The

latter is a very severe mathematical constraint and is unnecessary for this particular wave field. The beam need only be peaked in the direction of interest and minimal wherever else there is energy in the input wave field. If no energy exists in the range $-90^{\circ}<\theta<90^{\circ}$ for example, the beam may take on arbitrary values. The MLM beam pattern can be shown to be of the form:

$$B_{MLM}[\theta;\omega|\theta_o;\omega_o] = \frac{\sum_{m,n}^{N} E'_m(\theta)\, Q_{mn}(\omega)\, E_n(\theta_o)}{\sum_{m,n}^{N} E'_m(\theta_o)\, Q_{mn}(\omega)\, E_n(\theta_o)}$$

where $E_m(\theta)$ is $\{\exp(j\underset{\sim}{k}\cdot\underset{\sim}{r}_m)\}$, r_m is the radius to the array elements, the prime denotes complex conjugate, and $Q_{mn}(\omega)$ is the inverse of the covariance matrix $\|C_{ij}\|$ (Baggeror, 1976).

The following figures show selected MLM beam patterns for Geometry #1, i.e., the three element array shown in Appendix A, Figure A-1(a). The pattern for look angle θ_o multiplies the input spectrum and the result is integrated, as in Eq.(4.1), to obtain the estimate of the spectrum in the direction $\theta = \theta_o$. The synthesis techniques employed in these numerical examples are discussed in Chapter V. Figure IV-4 shows the beam pattern at four "look angles" (θ_o = 0°, 135°, 150°, and 180°) for the case of a plane wave of frequency ω = 0.2 rad. and incident angle θ = 150°. The beam patterns are plotted in decibels, i.e., 10 $\log_{10} B[\theta,\omega]$, on a linear scale every five degrees with the origin as -15db. A small arrow just outside the unit circle (0db) points (approximately) to the look angle θ_o. Also plotted are the spreading functions or normalized directional spectra for the input, the direct analysis, [Eq.(3.4)] and the MLM analysis [Eq.(3.5)]. The input here is a spatial delta function and is represented by a triangle of unit area and is drawn with a solid line. The direct spectral estimate is shown as a series of small triangles and is nearly a constant for this example. The MLM spectral estimate is shown as a solid line with "plus" signs.

Note that the beam pattern is unity (0db) in the θ_o direction as required by Eq. (4.3). Outside of θ_o, the beam pattern is effectively null in the input energy direction but can vary wildly otherwise. These

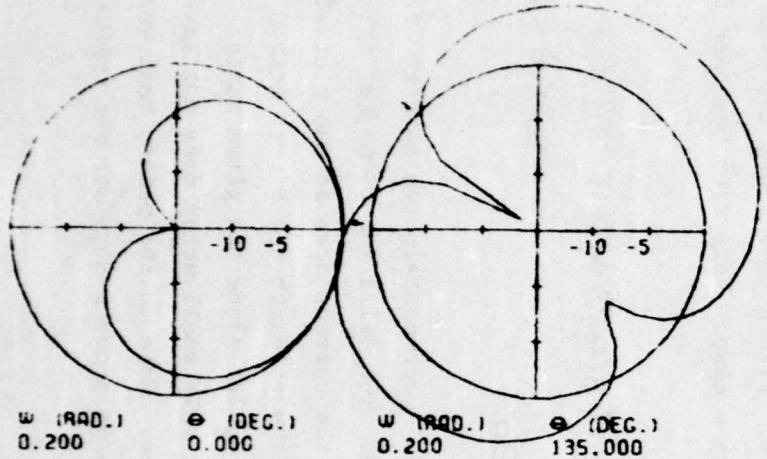

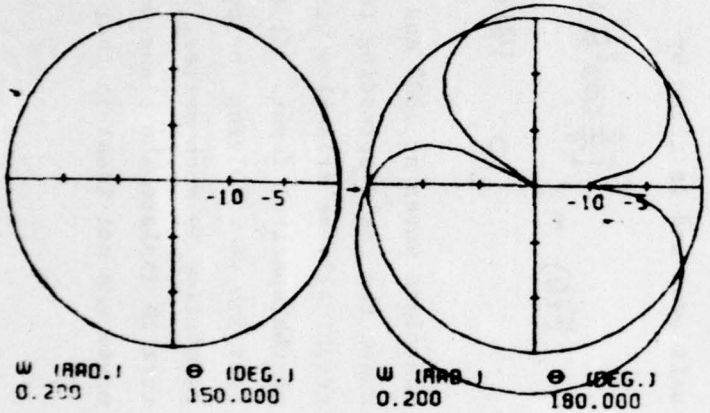

GEOMETRY NO. 1

BEAM PATTERNS IN DECIBELS (ORIGIN=-150B)

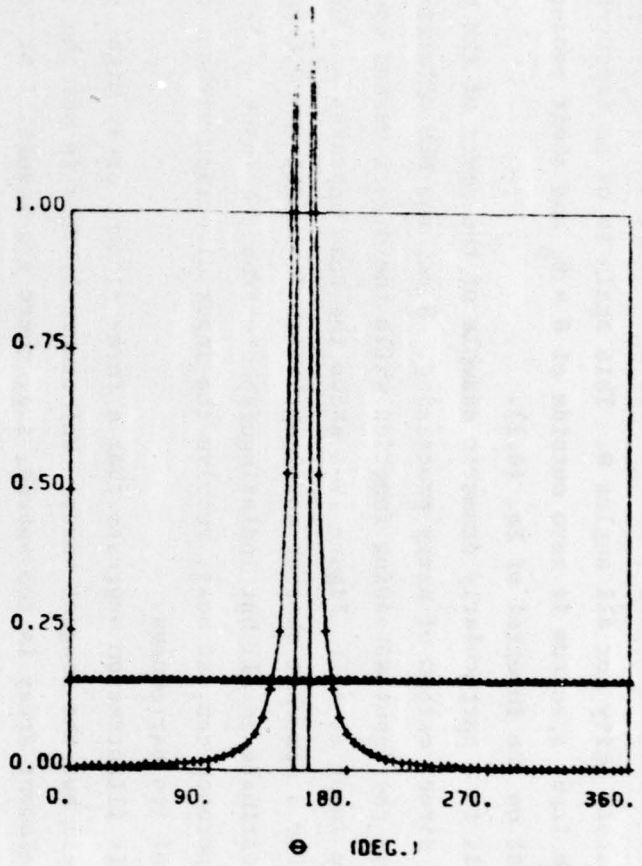

FIGURE IV-4

large variations "allow" the main lobe to be narrow but are of no other importance. Relatively little energy is "leaked" into the estimate of $S(\theta_o)$ from directions other than θ_o. For $\theta_o = 150°$, the beam pattern is approximately unity for all angles θ. This again is of no importance since the input spectrum is zero outside of $\theta = \theta_o$ and their product does not impact on the integral of Eq. (4.1).

This is a particularly dramatic example of the power of the MLM over the direct method of array processing. Here, the MLM effectively reproduces the input spreading function while the direct method cannot resolve the input at all. Figure IV-5 shows the beam patterns and normalized spectra for a somewhat shorter wavelength with frequency $\omega = 0.6$ radians. The MLM estimate is all but indistinguishable from the input while the direct approach can, at best, resolve the input direction without any measure of its narrowness.

This illustration suggests that a three element array might perfectly resolve all but the longest waves. Unfortunately this is not the case. A three element array is too sparse, i.e. there are insufficient terms in the Fourier series of Eq. (3.5), to describe a spreading function with a much more complicated structure. Figure IV-6 shows the beam patterns and spectral estimates for such a case. Here $F(\theta)$ has been normalized to unit area and is given by

$$F(\theta) = \begin{cases} \left[\frac{2}{\pi}\cos^2\theta + 0.1\left(\delta(100°) + \delta(150°)\right)\right]/1.2 & 90° < \theta < 270° \\ 0 & |\theta| < 90° \end{cases}$$

The plane waves at 100° and 150° each contain ten percent of the energy under the $\cos^2\theta$ spreading term. The delta functions $\delta(\theta)$ are presented graphically as triangles with the correct area at the plotted 5° spacing of the spectral input. At this wavelength the direct method does a very poor job of resolving the $\cos^2\theta$, let alone the plane waves. The MLM's resolution is much better, but this small array does not have the structure to isolate the plane waves. More to the point, real world measurements are not ideal in that large amounts of noise are typically present.

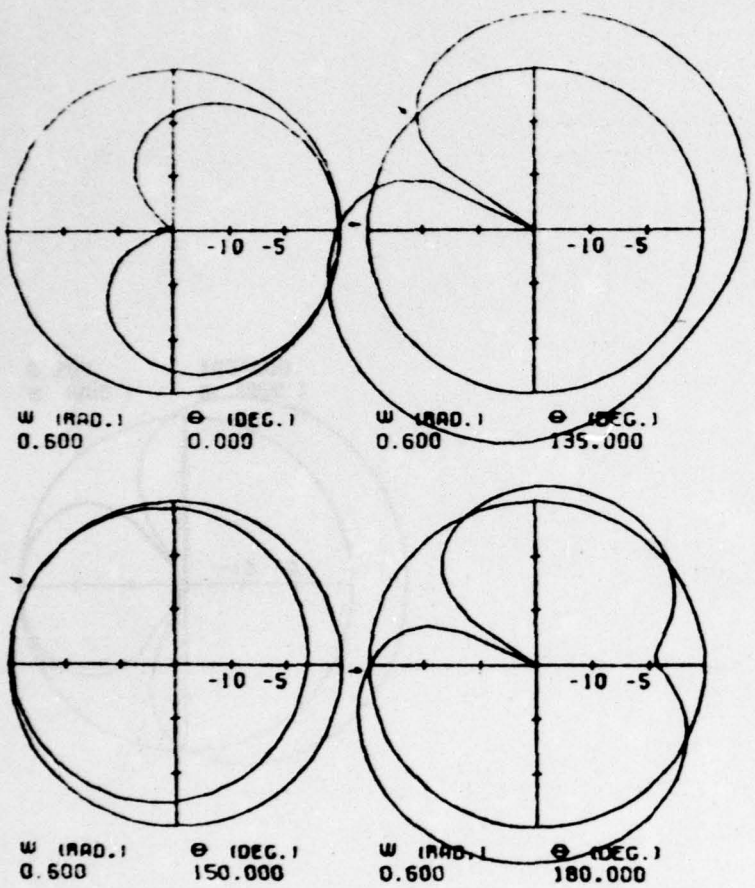

GEOMETRY NO. 1

BEAM PATTERNS IN DECIBELS (ORIGIN=-150B)

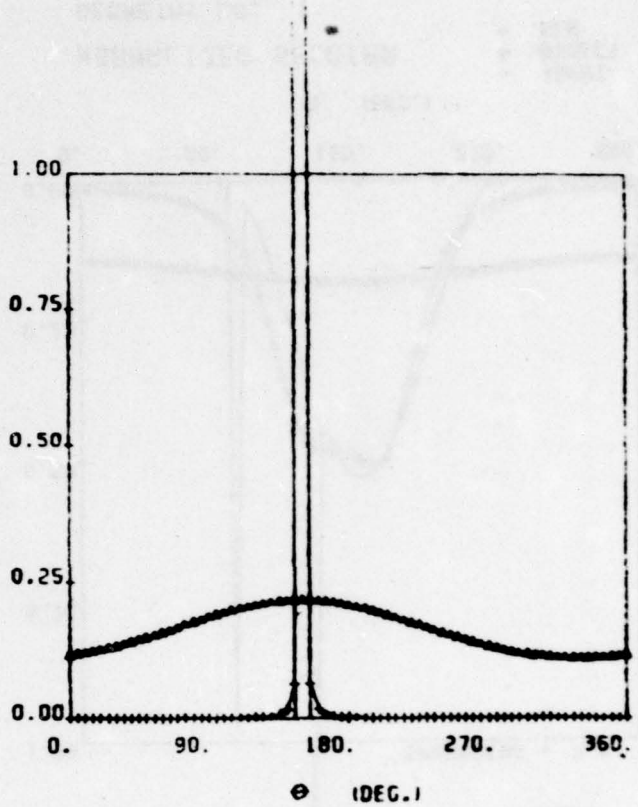

NORMALIZED SPECTRA

GEOMETRY NO. 1

ω (RAD.) = 0.600

NOISE (PERCENT): INSTR. 0.00
PROP. 0.00

FIGURE IV-5

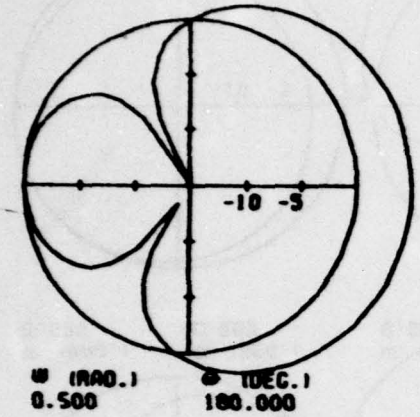

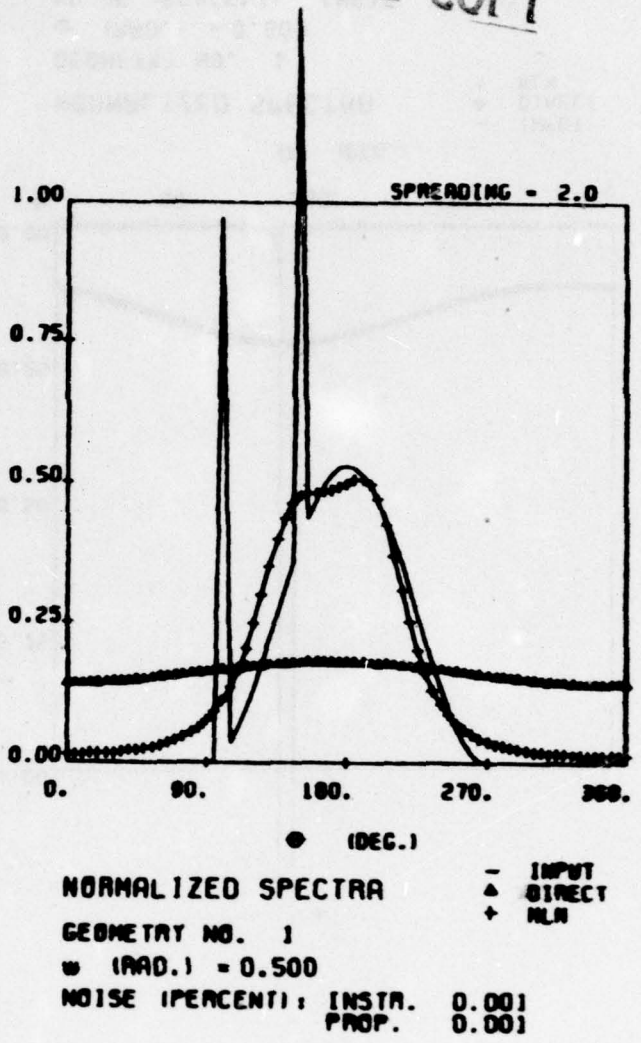

GEOMETRY NO. 1

BEAM PATTERNS IN DECIBELS (ORIGIN=-150θ)

FIGURE IV-6

These extraneous signals greatly reduce the MLM's ability to adapt to the data and result in significant reduction in spectral resolution. In order to analyze the effects of such things as wavelength, noise, and array geometry on the resolving ability of the MLM, a number of pertinent topics dealing with the simulation of real data are discussed in Chapter V.

V. THE COVARIANCE MATRIX, RESOLUTION, AND NOISE

Due to the nonlinear and adaptive character of the MLM, the amount of directional spectral "resolution" one might expect to achieve with a given system is difficult to quantify. Resolution depends on the array size and geometry, the frequency range, and the amount of "noise" introduced during the measurements and analysis. Analytical estimates of the importance of each of these factors are in general not available since the properties of the inverse cross-covariance matrix are not well known. In order to provide guidance for the design of array systems, it will be necessary to resort to numerical simulations of sample cross-covariance matrices for use with the maximum likelihood analysis. This will require the selection of representative directional spectral models, corrected for the effects of noise, and the taking of their spatial transforms.

1. Synthesis of the Covariance Function

The simplest ocean wave model is an infinitely long crested wave of length , amplitude A, and circular frequency ω moving in the θ direction, e.g., $\eta(t,\underline{x}) = A \cos(\underline{k} \cdot \underline{x} - \omega t)$ where $\underline{k} = [k\cos\theta, k\sin\theta]$ and $k(\omega)$ obeys the dispersion relationship. The directional spectrum is singular in frequency and direction and a particularly useful model for testing the limits of the type of resolution. A more realistic model of the sea surface is the multi-directional random wave model. The directional spectra referred to in this report are characterized by their separability into azimuth (θ) and frequency (ω). Although this choice is mathematically restrictive and does not conform to the spreading models suggested by Pierson(1976), it includes a sufficiently large number of instructive cases. By hypothesis, it is assumed that the directional spectrum $S(\omega,\theta)$ may be decomposed as

$$S(\omega,\theta) = S(\omega) F(\theta) \tag{5.1}$$

where the "spreading function" $F(\theta)$ embodies all the directionality of

$S(\omega,\theta)$ in the azimuth dependence θ and $S(\omega)$ contains all the frequency/wavelength character. Hence the spreading function $F(\theta)$, by definition, has the property that

$$\int_0^{2\pi} F(\theta)\, d\theta = 1. \tag{5.2}$$

The spatial covariance matrix $C(\omega,\underline{r})$ where $\underline{r}$ is the spatial lag, is given by the inverse spatial transform of the spectrum

$$C(\omega,\underline{r}) = \frac{S(\omega)}{2\pi} \int_0^{2\pi} F(\theta)\, e^{-j\underline{k}\cdot\underline{r}}\, d\theta. \tag{5.3}$$

Note that $\underline{k} \cdot \underline{r} = kr\cos(\theta - \phi)$ where $r = |\underline{r}|, \phi = \arg(\underline{r})$, and k is the wavenumber magnitude demanded by the dispersion relation. Since the interest here is in discrete arrays, the covariance function need be evaluated only at the array element pairs $\underline{r}_{ij} = \underline{x}_i - \underline{x}_j$, i.e.,

$$C_{ij}(\omega) = \frac{S(\omega)}{2\pi} \int_0^{2\pi} d\theta\, F(\theta)\, e^{jkr_{ij}\cos(\theta-\phi_{ij})} \tag{5.4}$$

and is referred to as the covariance or cross-covariance matrix. The temporal spectrum $S(\omega)$ is arbitrary and may be taken to be any desired point spectrum. Since the concern here is limited to the directional resolution of the array, the signal power can be normalized and the desired spreading function selected for each frequency. Formally, the spreading function $F(\theta)$ can be expanded in a Fourier series in θ, i.e.,

$$F(\theta) = \sum_{n=-\infty}^{\infty} a_n\, e^{-jn\theta} \tag{5.5}$$

where $\{a_n\}$ are the Fourier coefficients given by

$$a_n = \frac{1}{2\pi}\int_0^{2\pi} F(\theta)\, e^{jn\theta}\, d\theta. \tag{5.6}$$

Using the identity

$$\frac{1}{2\pi}\int_0^{2\pi} e^{-j(kr\cos(\theta-\varphi)+n\theta)}\, d\theta = e^{-jn(\varphi+\pi/2)} J_n(kr) \tag{5.7}$$

the covariance function becomes

$$C(\omega,\Sigma) = S(\omega)\sum_{n=-\infty}^{\infty} a_n e^{-jn(\varphi+\pi/2)} J_n(kr) \tag{5.8}$$

where the coefficients $\{a_n\}$ are given by Eq.(5.6). This form for $C(\omega,\underline{r})$, while instructive, is not necessarily computationally efficient and more direct schemes for its evaluation will be employed where expedient. Three types of spectral spreading functions and the resulting spatial covariance matrices are discussed in Appendix B, namely an omnidirectional, a raised cosine, and a delta function spectrum. These are sketched in Figure V-1 and are intended as basic examples of directional spectra for use in evaluating the resolution capabilities of various array geometries. These spreading functions are by no means exhaustive though various combinations of them yield an ample variety for present purposes.

2. Wavelength Resolution and Matrix Stability

The essential requirement for use of the maximum likelihood method of spectral estimation is the existence of the inverse (i.e., nonsingularity) of the covariance matrix $C_{ij}(\omega)$. In theory, any realizable propagating wave field will have a non-singular covariance matrix. Unfortunately, this is far from the case in terms of numerical stability. In fact, both the covariance matrix and its inverse rapidly become computationally singular as the array size to wavelength ratio tends to zero. This can be easily seen for the limiting case of a unidirectional wave

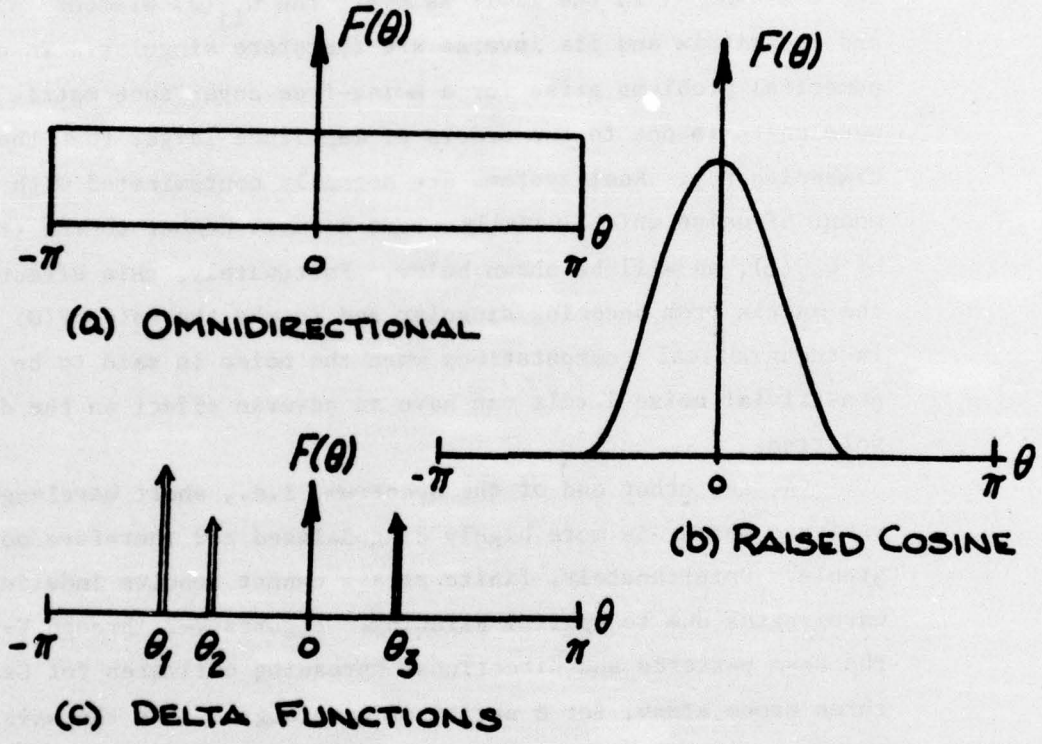

FIGURE V-1 Spreading Functions for Spatial Covariance Synthesis

train. The covariance matrix is obtained from Eq. (5.3) with elements

$$C_{ij}(\omega) = \frac{S(\omega)}{2\pi} e^{ikr_{ij}\cos(\theta - \phi_{ij})} \tag{5.9}$$

where $k = 2\pi/\lambda$. In the limit as $\lambda \to \infty$, the $C_{ij}(\omega)$ elements all become unity and the matrix and its inverse are therefore singular. In practice, numerical problems arise for a noise-free covariance matrix when the wavelength is one to two orders of magnitude larger than the typical array dimension r_{ij}. Real systems are normally contaminated with a certain amount of noise which usually adds a small number to the (real) diagonal of $C_{ij}(\omega)$, as will be shown below. Fortunately, this effectively prevents the matrix from becoming singular and is why the value $F(\theta) \times 10^{-5}$ is used in the numerical computations when the noise is said to be zero. However, non-trivial noise levels can have an adverse effect on the directional resolution.

At the other end of the spectrum, i.e., short wavelengths, the covariance matrix is more highly diagonalized and therefore more numerically stable. Unfortunately, finite arrays cannot resolve indefinitely short wavelengths due to spatial aliasing. Figures V-2 through V-5 again show the beam patterns and directional spreading estimates for Geometry #1, the three probe array, for a series of wavelengths. As the wavelength becomes shorter, the MLM beam pattern exhibits more structure and is thus able to follow more closely the actual spreading function. This is also true for the direct method, Equation (3.4), but there is an increasing number of ambiguous peaking. In the final figure, the frequency is 2.8 rad. and the wavelength is only about half the average radius of the array elements and less than one third of the gage pair distances. The direct spectral estimate has completely degenerated and the MLM has shown signs of numerical instability.

A consideration of the beam pattern will help to explain the degenerate performance of the array at the shorter wavelengths. The expression for the natural beam pattern will be used in the following discussion, though the conclusions will later be seen to apply to the MLM beam patterns

as well. The natural beam pattern for an N element array is given by Equation (4.5). An equivalent form of the summand is

$$e^{j\frac{2\pi}{\lambda} r_{ij} \cos(\theta-\theta_o-\phi_{ij})} \tag{5.10}$$

where λ is the wavelength and (r_{ij}, ϕ_{ij}) are the polar coordinate distances between the i-j gage pair. A Fourier series expansion for the real part of this expression may be written as

$$J_o\left(\frac{2\pi r_{ij}}{\lambda}\right) + 2\sum_{k=1}^{\infty}(-1)^k J_{2k}\left(\frac{2\pi r_{ij}}{\lambda}\right)\cos(2k\theta - 2k(\theta_o-\phi_{ij})) \tag{5.11}$$

where the Fourier coefficients, $J_{2k}(2\pi r_{ij}/\lambda)$ are the n^{th} order Bessel functions. For long wavelengths, where $2\pi r_{ij}/\lambda \ll 1$, the series converges very rapidly since the coefficients fall off as

$$J_{2k}\left(\frac{2\pi r_{ij}}{\lambda}\right) \simeq \frac{(2\pi r_{ij}/\lambda)^{2k}}{2^{2k}(2k)!}, \quad k=0,1,2,\ldots \tag{5.12}$$

However, as r_{ij}/λ approaches unity, the Bessel functions behave as:

$$J_{2k}(2\pi r_{ij}/\lambda) \simeq \frac{1}{\pi}\sqrt{\frac{\lambda}{r_{ij}}}\cos\left(\frac{2\pi r_{ij}}{\lambda} - k\pi - \frac{\pi}{4}\right), \; k=0,1,\ldots \tag{5.13}$$

The series coefficients are now comparable in size and the pattern becomes highly structured in angle θ, i.e., the pattern oscillates wildly for small intervals about $\theta=\theta_o-\phi_{ij}$. Thus, the beam pattern begins to degenerate or become "hashy" if more than a few of the interprobe spacings r_{ij} become comparable to a wavelength. This effect is generally referred to as spatial aliasing. The interprobe spacing for Geometry #1, for example, is approximately 87 feet. In Figure V-2, $r_{ij}/\lambda = 0.43$ and some rippling of the direct spectral estimate is apparent. In Figure V-3, $r_{ij}/\lambda = 1.55$ and the disastrous effects of aliasing on the direct method are evident.

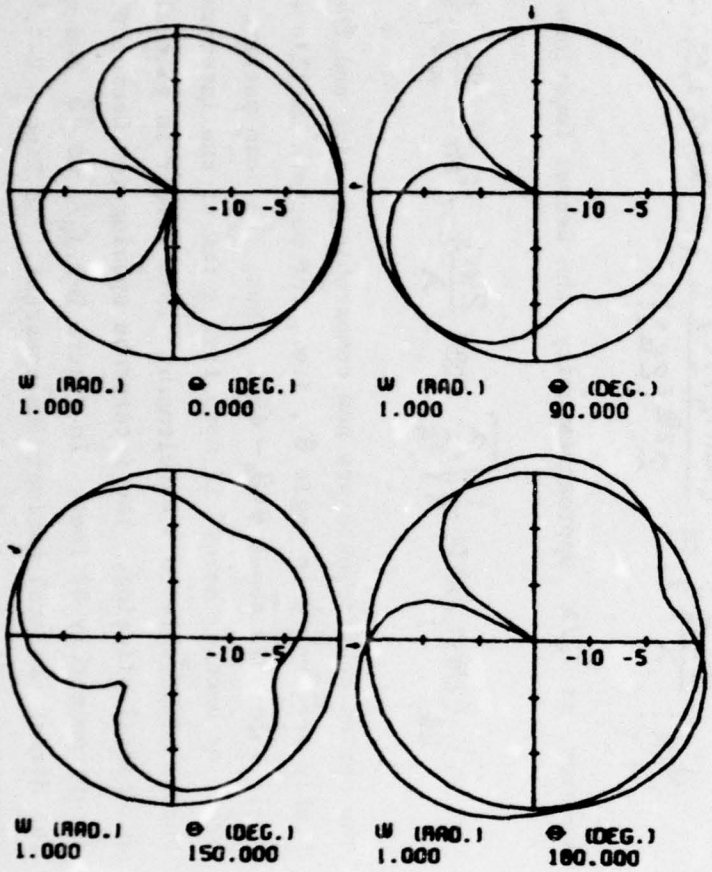

GEOMETRY NO. 1

BEAM PATTERNS IN DECIBELS (ORIGIN=-150B)

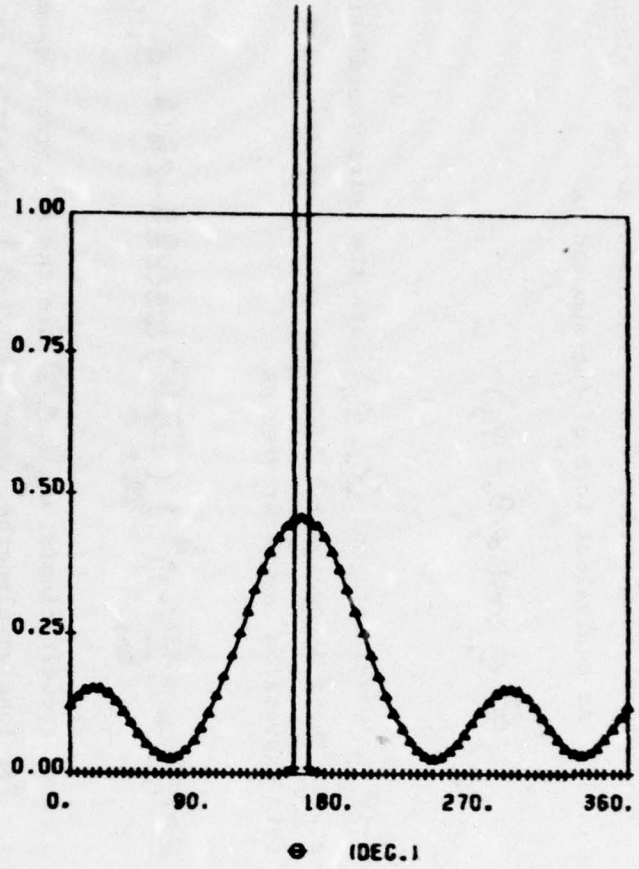

NORMALIZED SPECTRA

– INPUT
▲ DIRECT
+ MLM

GEOMETRY NO. 1

w (RAD.) = 1.000

NOISE (PERCENT): INSTR. 0.001
PROP. 0.001

FIGURE V-2

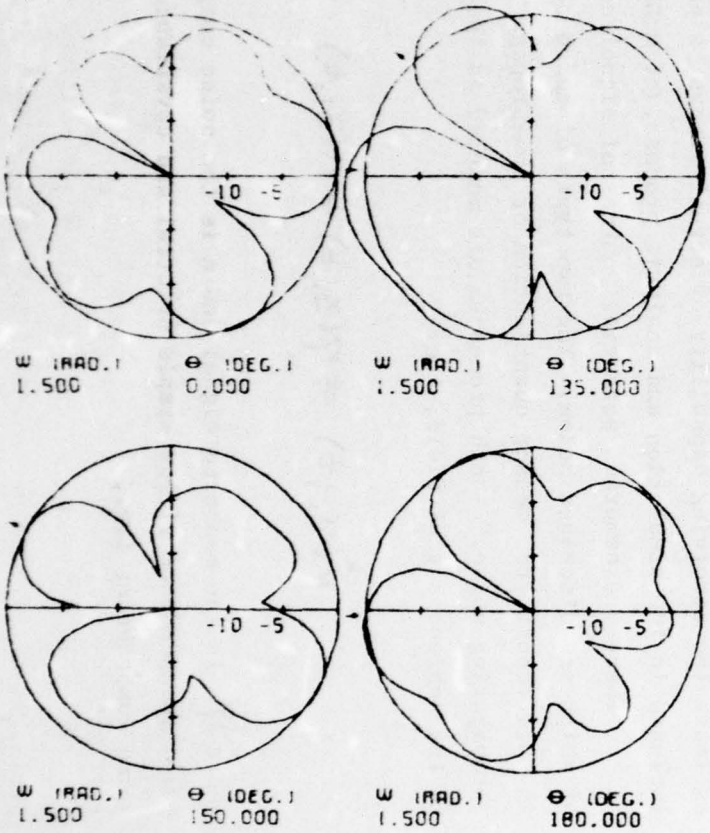

GEOMETRY NO. 1

BEAM PATTERNS IN DECIBELS (ORIGIN=-15DB)

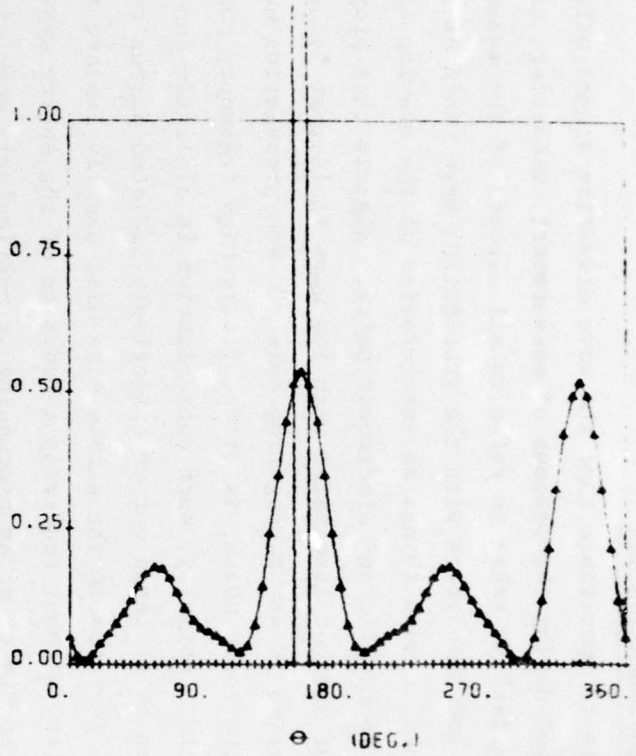

NORMALIZED SPECTRA

GEOMETRY NO. 1

ω (RAD.) = 1.500

NOISE (PERCENT): INSTR. 0.00
PROP. 0.00

FIGURE V-3

3. Noise Contamination

It is inevitable that the wave elevation signal will be contaminated by "noise" during the process of measurement, recording, and/or processing. Here, "noise" is taken to refer to all aspects of the measurement analysis not associated with the propagating wave field of interest. These would include such things as inaccuracies of the sensing elements, quantization, round-off, and electronic noise. Signals that propagate across the array but are not associated with the wave field that is being measured are referred to as "propagating noise." Non-propagating noise, such as 60cps electronic noise, is often of very high frequency compared to the wave field. Normally, such contamination is of little concern. The noise can often be filtered out or effectively isolated during the processing. A simple increase in the sample size will usually improve the statistical reliability without requiring a redesign of the entire system. Unfortunately, the MLM of array processing is particularly sensitive to the quantity of noise. A noise-to-signal ratio of even a few percent can greatly reduce the angular resolution of the small arrays in question. In order to estimate the resolving capability of actual arrays, a noise model must be included in the simulation and analysis process, (cf McDonough, 1972).

There are numerous potential sources of signal contamination, some of which are discussed below. The two types of noise actually addressed in this report are "sensor quantization or non-propagating noise" and "propagating noise." Both processes are modeled as independent additions to the ambient signal field, i.e.,

$$\hat{\eta}(\underset{\sim}{x}_i, t) = \eta(\underset{\sim}{x}_i, t) + n(\underset{\sim}{x}_i, t) \tag{5.14}$$

where $\hat{\eta}$ is the measured signal and n is the noise component. This assumed independence yields simple spectral and covariance addition of the noise components, i.e.,

$$\hat{S}(\omega) = S_\eta(\omega) + S_n(\omega), \tag{5.15a}$$

$$\hat{C}(\omega, \xi_{ij}) = C_\eta(\omega, \xi_{ij}) + C_n(\omega, \xi_{ij}). \tag{5.15b}$$

The essential problem now is to obtain an estimate of the signal-to-noise ratio and covariance function of actual array systems.

High Frequency Noise

Wave frequencies above the bandwidth of interest and high frequency electronic noise can pose serious aliasing problems if they are not effectively filtered out of the signal. This is normally done prior to A/D conversion; otherwise the filtering must be done digitally with a much finer time step than is required for the spectral analysis. Since such filtering is normally employed, frequency aliasing will not be discussed further. The problem of spatial or wavenumber aliasing will be addressed below.

Propagating Noise

Propagating noise refers to any signal that is coherent across the array yet is not part of the wave field of interest. The major source of propagating noise for a fixed array is likely to be the reflections from local structures. These reflected waves represent spatially inhomogeneous signals that are processed like any other propagating signal. The interpretation of the measured directional spectrum as a spatially stationary process may not be possible if there is a great deal of local interference. The spectral representation of locally generated (inhomogeneous) wave fields will likely be highly inaccurate due to the sparseness of the arrays in question.

The only propagating noise component of the synthesized signal will be an omnidirectional term. There appears to be no evidence that might suggest a significant amount of naturally occurring wave energy distributed uniformly in azimuth. The directional spreading could, of course, be very broad and contain numerous humps; nevertheless, the truly omnidirectional

component is assumed to be small and essentially uncorrelated with the principal wave field of interest. As shown above, a uniform spreading function $F_n(\theta) = 1/2\pi$ yields a cross-covariance term of the form

$$C_n(\omega, r_{ij}) = N(\omega) J_o(k r_{ij})$$

where $N(\omega)$ is the noise power level and $J_o(.)$ is the zero order Bessel function. In Chapter VI it will be shown that omnidirectional (propagating) noise appears to be treated like any other propagating signal by the MLM processing scheme.

Field Noise

The desired wave field signal is often contaminated with random signals due to spray, wave breaking, sheltering and reflections from local structures, water runoff from the sensors, etc. These events may yield a (noticeable) contribution over a broad band of frequencies but should only be weakly correlated across the array. Their effect on the maximum likelihood processing is most pronounced when the wave amplitudes are small and there is a significant noise-to-signal ratio. A priori estimates of the magnitude of the noise power are difficult to make. Most wave height sensors peform some filtering and are poorly responsive to the effects of spray and wave breaking. Water runoff can introduce a lag in the measured signal and distort the peaks. One would not expect these to be particularly serious problems, however.

On the other hand, contaminating waves generated by local structures may vary significantly in amplitude as they cross the array. Local reflections and sheltering could also yield signals that would not be uniformly coherent across the array.

Quantizing Noise

Quantizing errors can arise when a continuous variable is handled in a discrete form. Round-off errors in the course of digital signal processing on a mini-computer are an example. In most situations machine round-

off errors are not significant or can be reduced by going to higher precision. A more relevant example is the quantizing effects of a pin type wave detector as used in the San Francisco Bay experiments, (Chou, et al, 1974). This type of wave probe is able to resolve wave elevations only to within the pin spacing, Δp, on the staff. This anomaly may be modeled as a type of wideband sensor noise which effects only the diagonal of the covariance matrix $\| C_{ij}(\omega) \|$. For portions of the input spectrum with component amplitudes several times greater than the pin spacing width "Δp" it may be shown that for a wave sampling rate Δt, an effective noise power $\Delta p^2/12\Delta t$ is added to the main diagonal, $C_{ii}(\omega)$, of the covariance matrix. This result is based on the assumptions that 1) the uncertainty between the true and measured wave elevation is uniformly distributed over the spacing width Δp 2) that the sampling rate is on the order of the "Nyquist" rate (i.e., the reciprocal of twice the highest significant frequency component in the spectrum), and 3) the quantization uncertainties between wave probes are uncorrelated. Thus, for this type of wave probe the noise matrix is

$$\| N \| = \text{diag} \{ \Delta p^2/12\Delta t \}.$$

An expression of the percentage noise is given by:

$$\% = \frac{\Delta p^2/12\Delta t}{\frac{1}{2\pi}\int S(\omega)\,d\omega} \times 100$$

and for typical values of say $\Delta p = 1"$, $\Delta t = (1/2 \times 2.5$ cps) and very small waves, i.e., $(2\pi)^{-1}\int S(\omega)d\omega = 0.125\,\zeta^2$ the percentage error is found from the above expression to be 2.3%. A well designed system will therefore see at most a few percent quantizing noise for the smallest waves and considerably less for the design situation.

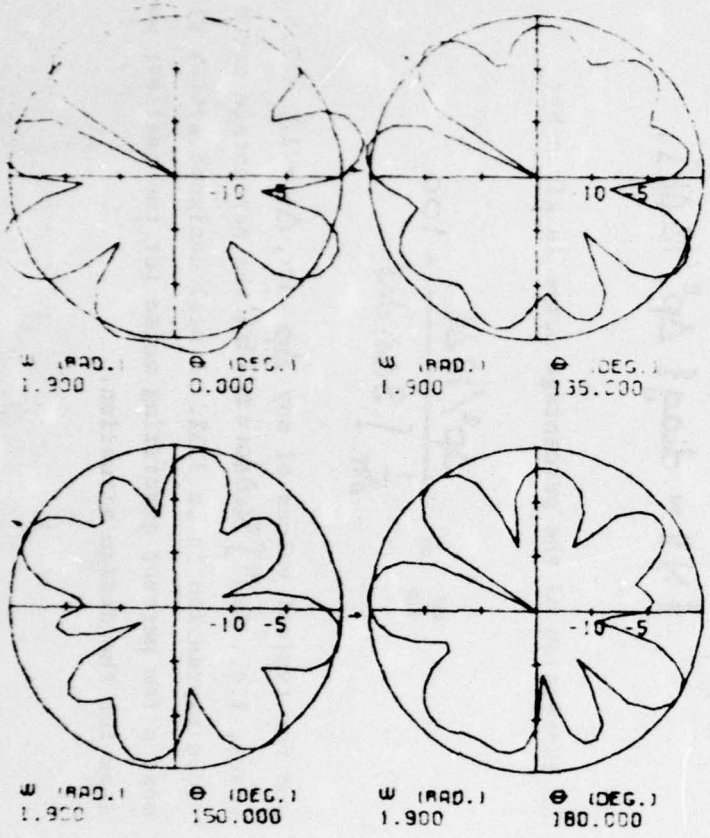
-10
-5
10
5
ω (RAD.)
1.900
θ (DEG.)
0.000
ω (RAD.)
1.900
θ (DEG.)
135.000
-10 -5
-10 -5
ω (RAD.)
1.900
θ (DEG.)
150.000
ω (RAD.)
1.900
θ (DEG.)
180.000
GEOMETRY NO. 1
BEAM PATTERNS IN DECIBELS (ORIGIN=-150)

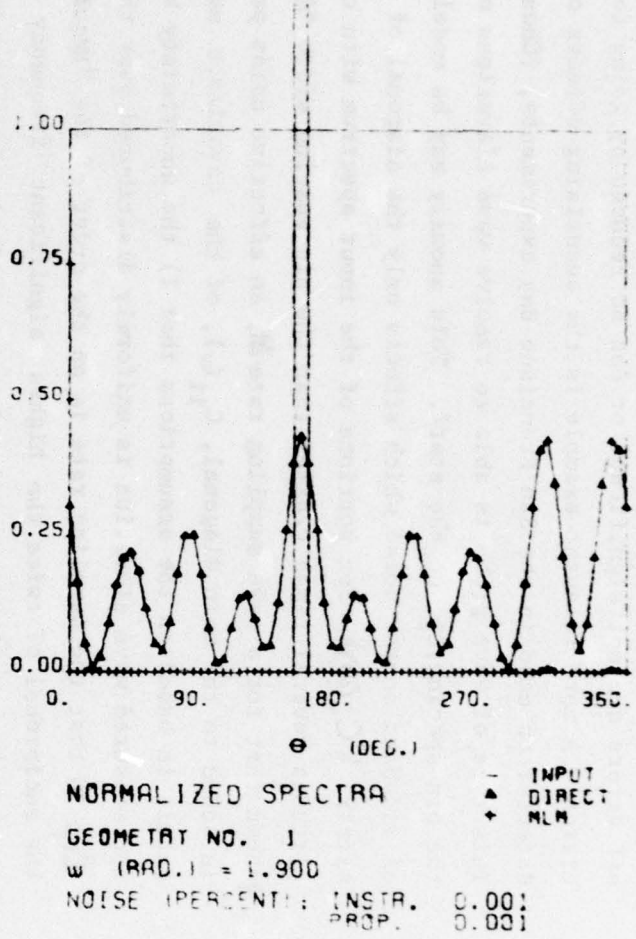
1.00
0.75
0.50
0.25
0.00
0.
90.
180.
270.
360.
θ (DEG.)
INPUT
DIRECT
MLM
NORMALIZED SPECTRA
GEOMETRY NO. 1
ω (RAD.) = 1.900
NOISE (PERCENT): INSTR. 0.00
PROP. 0.00

FIGURE V-4

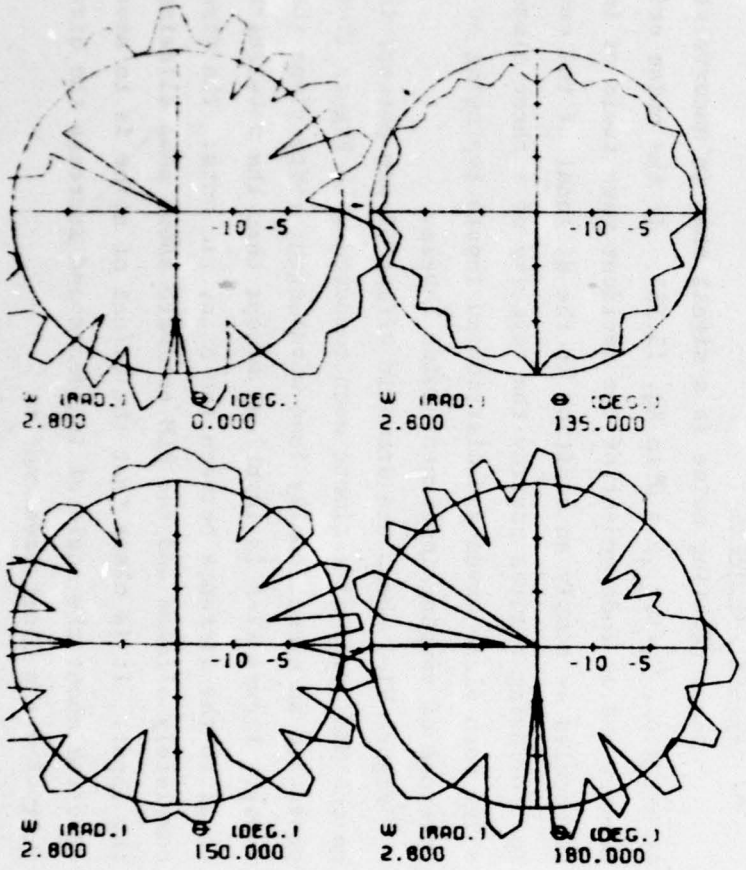

GEOMETRY NO. 1

BEAM PATTERNS IN DECIBELS (ORIGIN=-15DB)

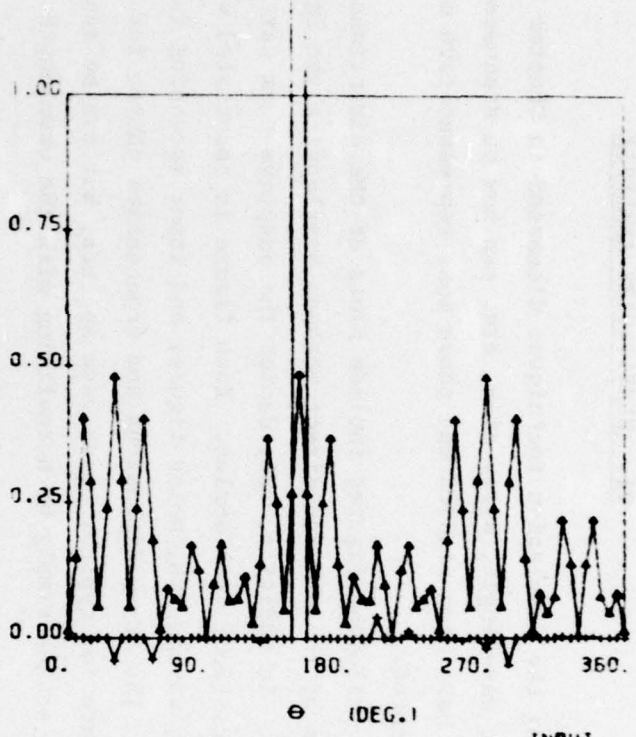

NORMALIZED SPECTRA

GEOMETRY NO. 1

ω (RAD.) = 2.800

NOISE (PERCENT): INSTR. 0.001
PROP. 0.001

FIGURE V-5

VI. SENSITIVITY ANALYSIS

Using the simulation techniques discussed in Chapter V, the effects of noise, wavelength, array size, etc. can now be discussed. Numerous examples have been studied and those most representative or illuminating are presented.

The following figures include plots of the directional spectral estimates of the MLM and direct methods overlapping the input spreading function. In addition, they depict the adaptive beam pattern of the MLM at four distinct look angles. Each figure is associated with distinct geometry, wavelength, noise figure, and input spreading function (cf Chapter IV). The array dimensions and frequencies chosen for presentation are appropriate for typical ocean wave spectra, but can be easily transferred to other scales simply by normalizing with the wavelength.

1. Noise, Wavelength, and Aliasing

a) Instrument Noise

Nonpropagating noise is a signal that is uncorrelated across the array, i.e., $C_n(\omega,\underline{r}_{ij}) = 0^*$ in Eq. (5.15). If the noise originates in the sensors and is independent of the incident wave field of interest, it can be modeled as simply an addition to the diagonal of the covariance matrix. The following figures portray the capacity of a three element array to resolve both plane waves and distributed inputs impinging on the array in the presence of varying instrument noise levels.

Figure VI-1 shows the dramatic effect of one percent instrument noise on the MLM spectral estimate when compared with Figure IV-4. This corresponds to an exceptionally long wavelength; fifty times the radius of the array. Figure VI-2 is identical except that the wavelength is now about equal to the distance between the array elements. The direct estimate is completely aliased and the MLM estimate shows some aliasing at 180° from the input. It is clear that the effect of noise is to smear the true spectrum about the angle of incidence and increase the directional ambiguity for the short wavelengths.

* $(i \neq j)$

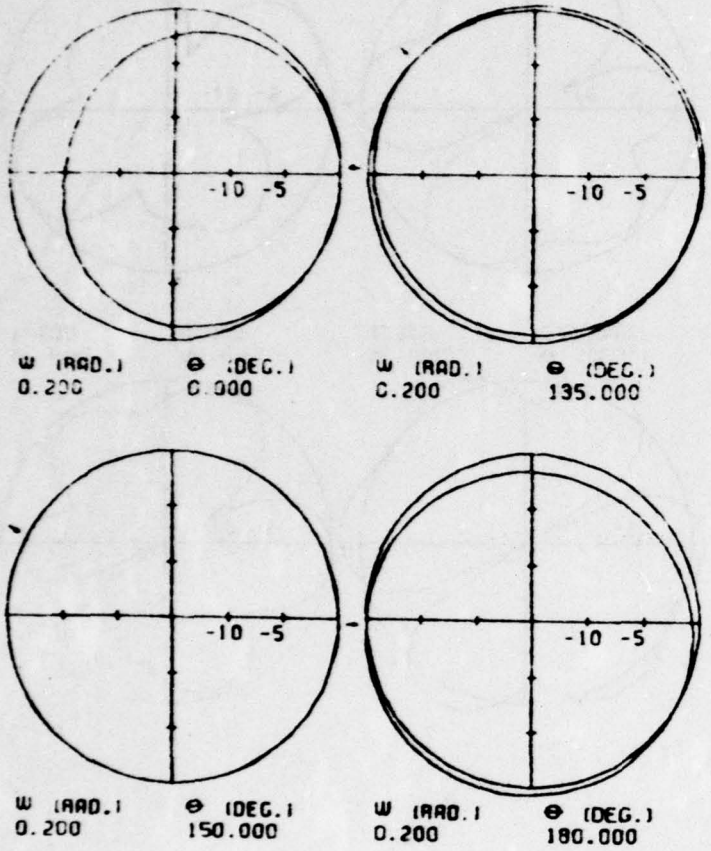

GEOMETRY NO. 1

BEAM PATTERNS IN DECIBELS (ORIGIN=-150B)

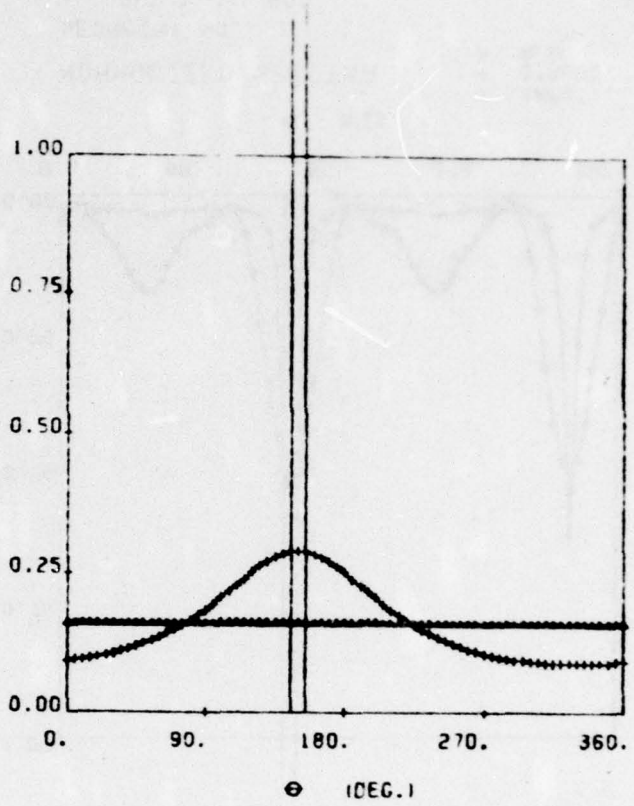

FIGURE VI-1

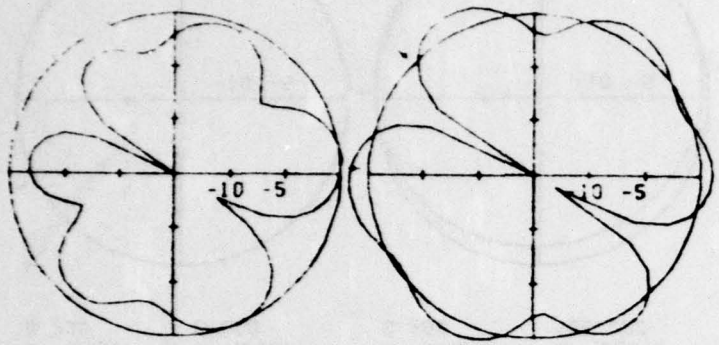

ω (RAD.) 1.500 Θ (DEG.) 0.000 ω (RAD.) 1.500 Θ (DEG.) 135.000

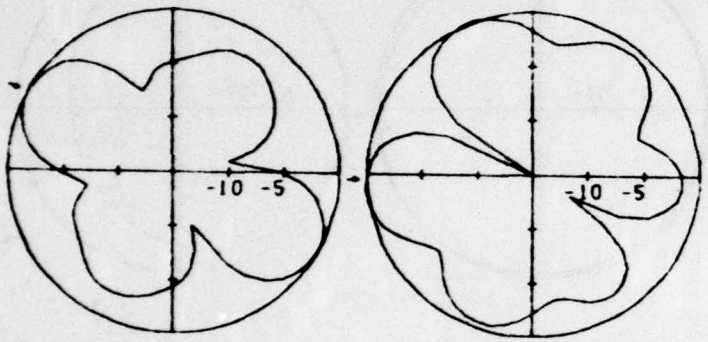

ω (RAD.) 1.500 Θ (DEG.) 150.000 ω (RAD.) 1.500 Θ (DEG.) 180.000

GEOMETRY NO. 1

BEAM PATTERNS IN DECIBELS (ORIGIN=-15DB)

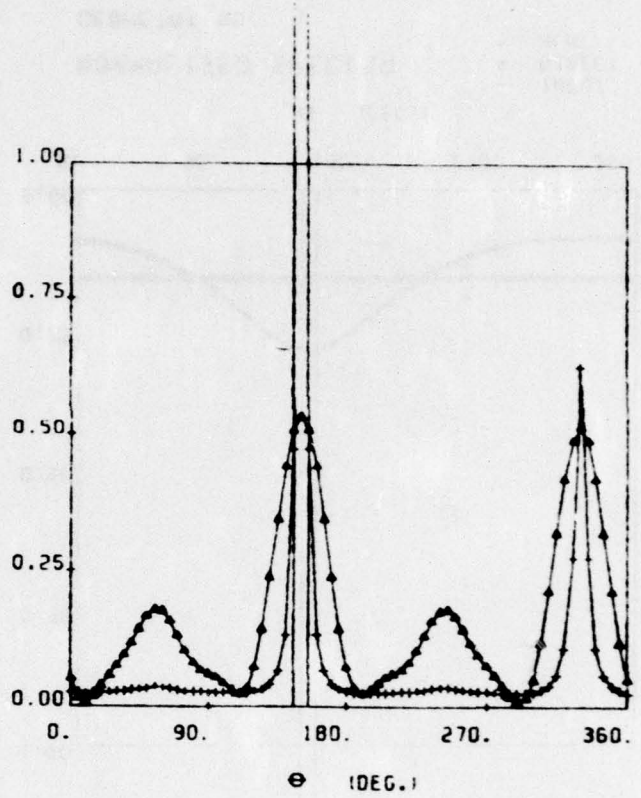

NORMALIZED SPECTRA

GEOMETRY NO. 1

ω (RAD.) = 1.500

NOISE (PERCENT): INSTR. 1.000
PROP. 0.001

FIGURE VI-2

Figures VI-3 through VI-5 are again for a single plane wave input at $\theta = 150°$ and various wavelengths, but the instrument noise level is now ten percent of the plane wave energy. It is clear that some care must be taken in estimating the input spectral width on the basis of either the direct of MLM estimates for such a small array. Figure VI-4 shows slight aliasing of the MLM estimate and Figure VI-5 has slightly increased aliasing over the one percent case of Figure VI-2.

Figure VI-6 through VI-10 are examples of the three element array's resolution for a more complicated input. Here, the spreading function $F(\theta)$ includes two plane waves and a cosine squared distribution. The plane waves are each ten percent of the energy of the cosine spreading function. None of the examples exhibit much ability to resolve the plane waves and the high frequency case ($\omega = 1.5$ rad) has degenerated entirely. Hence, the high frequency limit of the analysis depends not only on the wavelength and array geometry, but on the character of the spreading function.

It has been suggested that noise levels could be considerably larger than the one and ten percent that have been shown so far. Consider, for example, a six element array (Geometry #3) with $\omega = 0.8$ radians and a cosine spreading function raised to the fifieth power, i.e.,

$$F(\theta) = \alpha \cos^{50}\theta, \quad |\theta - 180°| \leq 90°.$$

Figures VI-10a, 10b, and 10c show the spectral estimates for instrument noise levels of 50, 100, and 200% of $F(\theta)$. In each case, the spectral peak has been noticeably lowered, largely due to an apparent increase in an omnidirectional component. If the omni-directional component is removed, the remaining estimate is still wider than the input spreading function. For the 200% noise level in particular, a fit to the modified MLM spectral estimate, i.e., $S_{MLM}(\theta) - S_{MLM}(0°)$, requires a cosine raised only to the eleventh power, rather than the fifty of the input. The beam patterns for these examples are very broad and are the cause of the poor resolution.

Figure I-2 is the MLM estimate of "cross-sea" data discussed in Chapter I. Two wave systems were generated in different regions and radiated

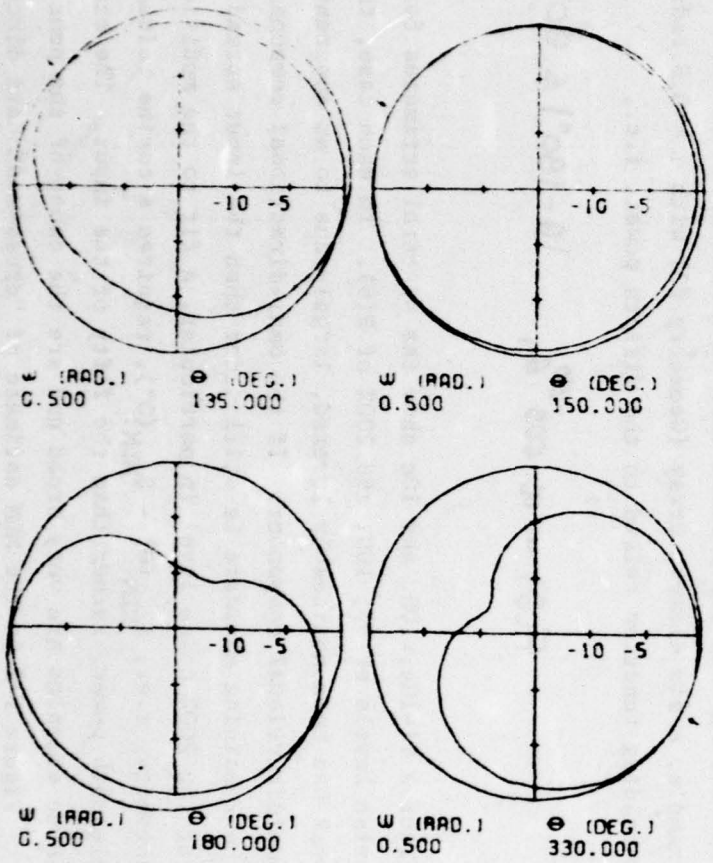

GEOMETRY NO. 1

BEAM PATTERNS IN DECIBELS (ORIGIN=-150B)

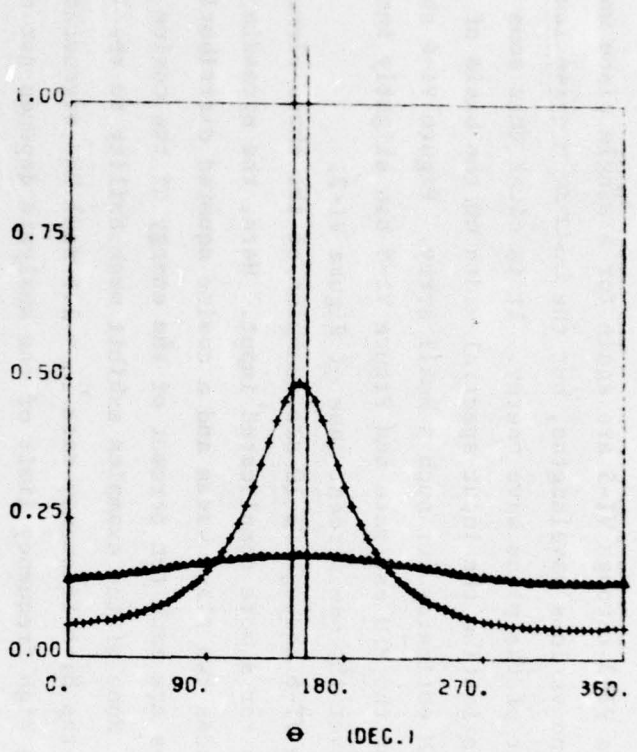

NORMALIZED SPECTRA

GEOMETRY NO. 1

ω (RAD.) = 0.500

NOISE (PERCENT): INSTR. 10.000
PROP. 0.001

FIGURE VI-3

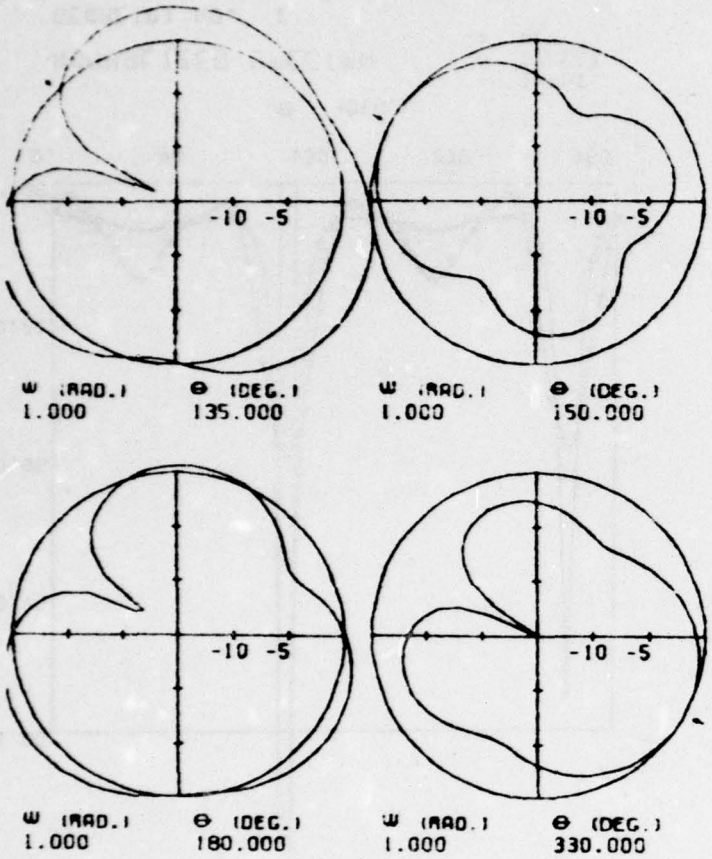
-10 -5
-10 -5
ω (RAD.)
1.000
Θ (DEG.)
135.000
ω (RAD.)
1.000
Θ (DEG.)
150.000
-10 -5
-10 -5
ω (RAD.)
1.000
Θ (DEG.)
180.000
ω (RAD.)
1.000
Θ (DEG.)
330.000
GEOMETRY NO. 1
BEAM PATTERNS IN DECIBELS (ORIGIN=-150B)

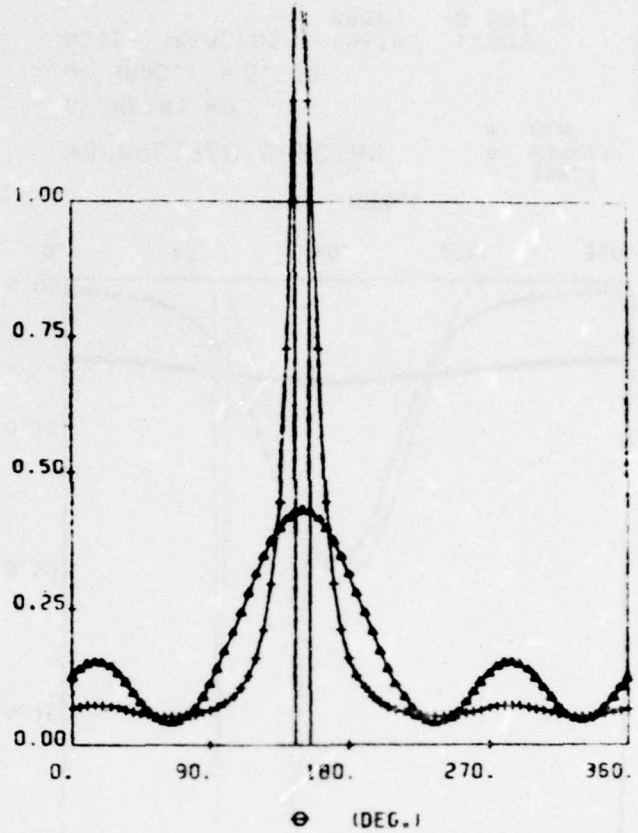
1.00
0.75
0.50
0.25
0.00
0.
90.
180.
270.
360.
Θ (DEG.)
NORMALIZED SPECTRA
INPUT
DIRECT
MLM
GEOMETRY NO. 1
ω (RAD.) = 1.000
NOISE (PERCENT): INSTR. 10.000
PROP. 0.001

FIGURE VI-4

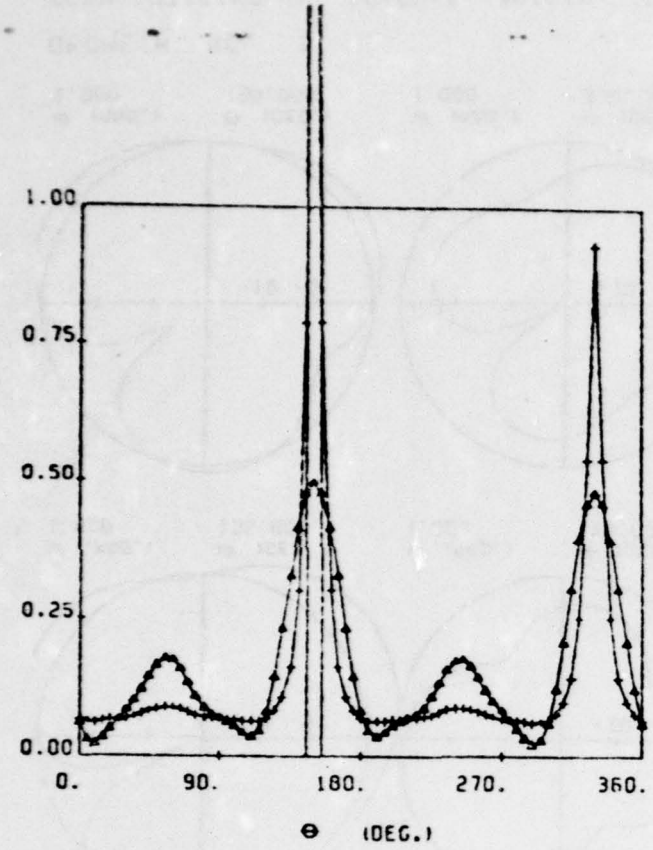

FIGURE VI-5

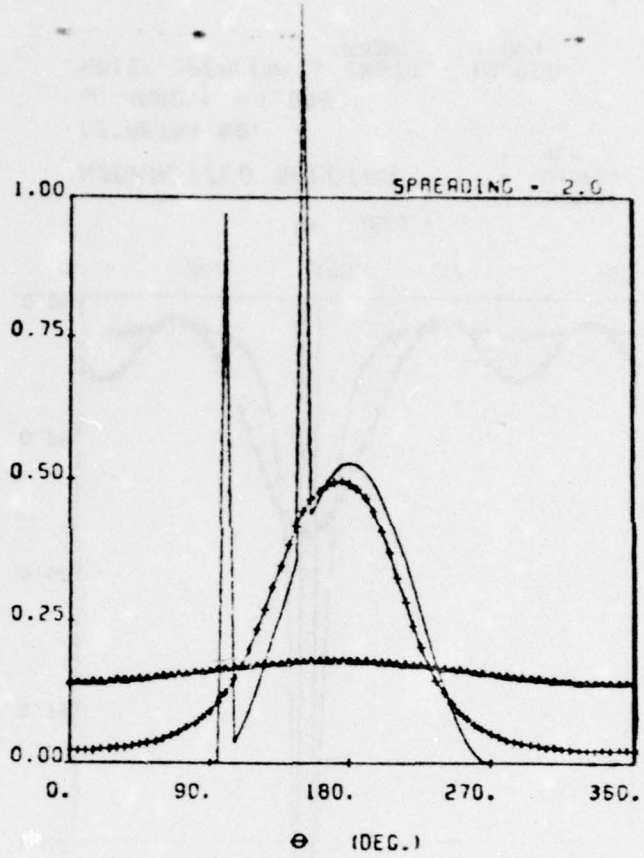

FIGURE VI-6

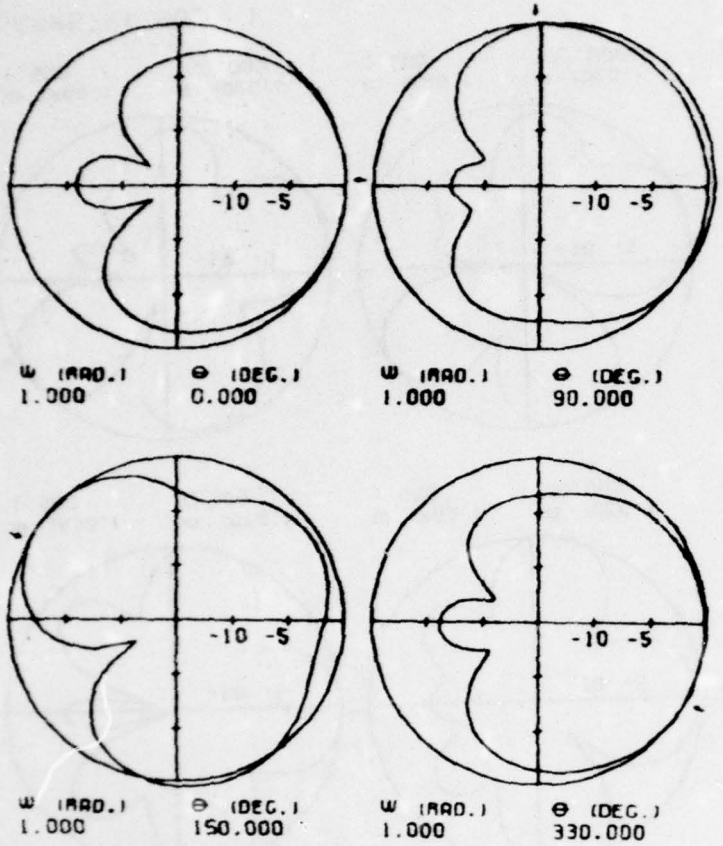
-10 -5
-10 -5
-10 -5
-10 -5
ω (RAD.)
1.000
Θ (DEG.)
0.000
ω (RAD.)
1.000
Θ (DEG.)
90.000
ω (RAD.)
1.000
Θ (DEG.)
150.000
ω (RAD.)
1.000
Θ (DEG.)
330.000
GEOMETRY NO. 1
BEAM PATTERNS IN DECIBELS (ORIGIN=-150B)

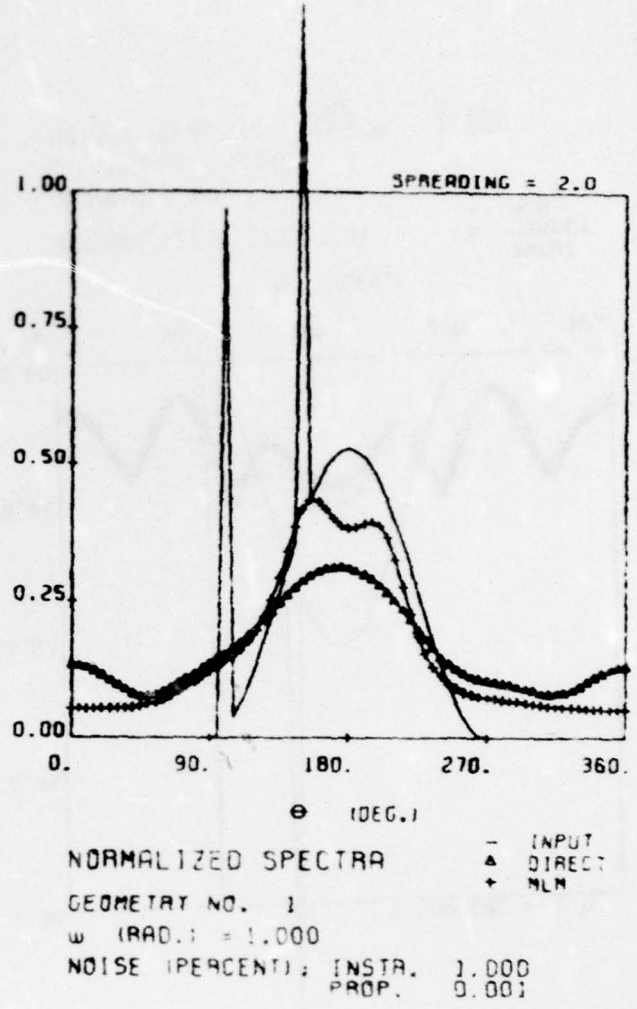
SPREADING = 2.0
1.00
0.75
0.50
0.25
0.00
0.
90.
180.
270.
360.
Θ (DEG.)
NORMALIZED SPECTRA
INPUT
DIRECT
MLM
GEOMETRY NO. 1
ω (RAD.) = 1.000
NOISE (PERCENT): INSTR. 1.000
PROP. 0.001

FIGURE VI-7

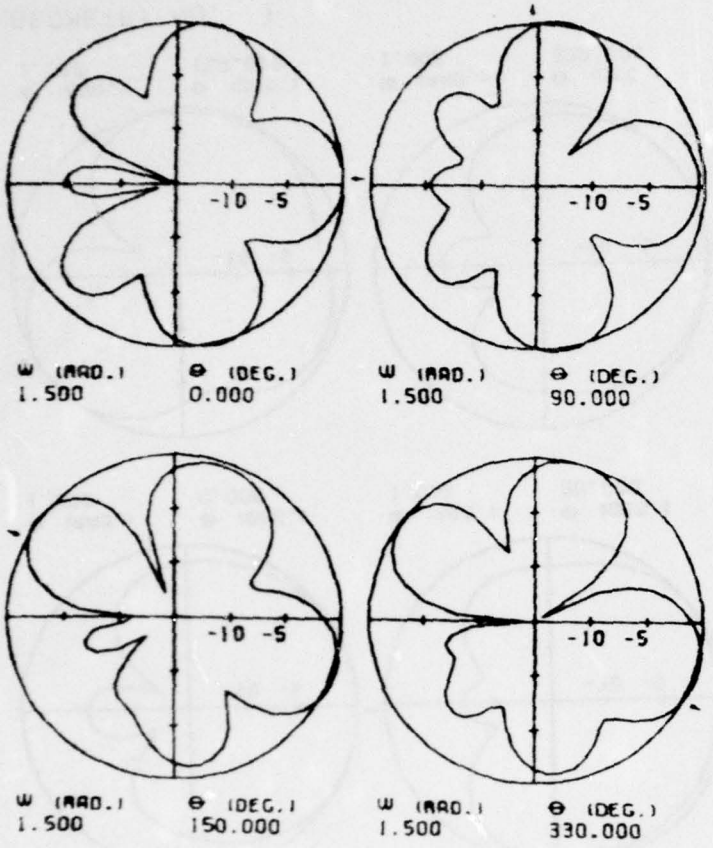

GEOMETRY NO. 1

BEAM PATTERNS IN DECIBELS (ORIGIN=-150B)

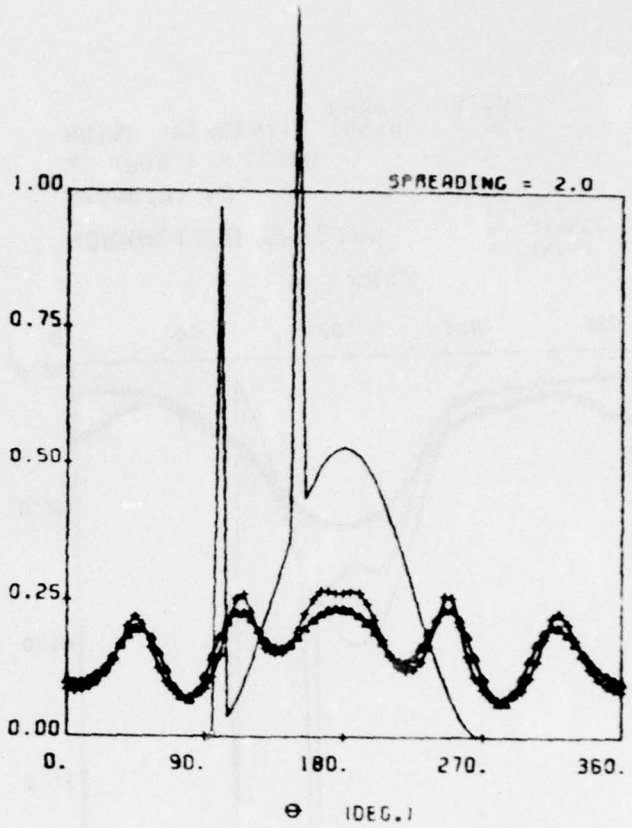

NORMALIZED SPECTRA

GEOMETRY NO. 1

ω (RAD.) = 1.500

NOISE (PERCENT): INSTR. 1.000
PROP. 0.001

FIGURE VI-8

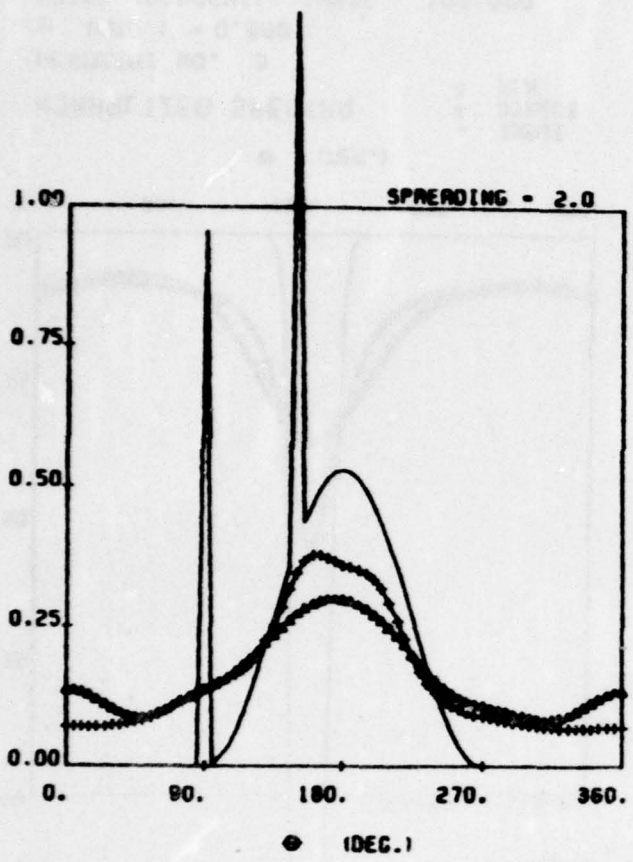

FIGURE VI-9

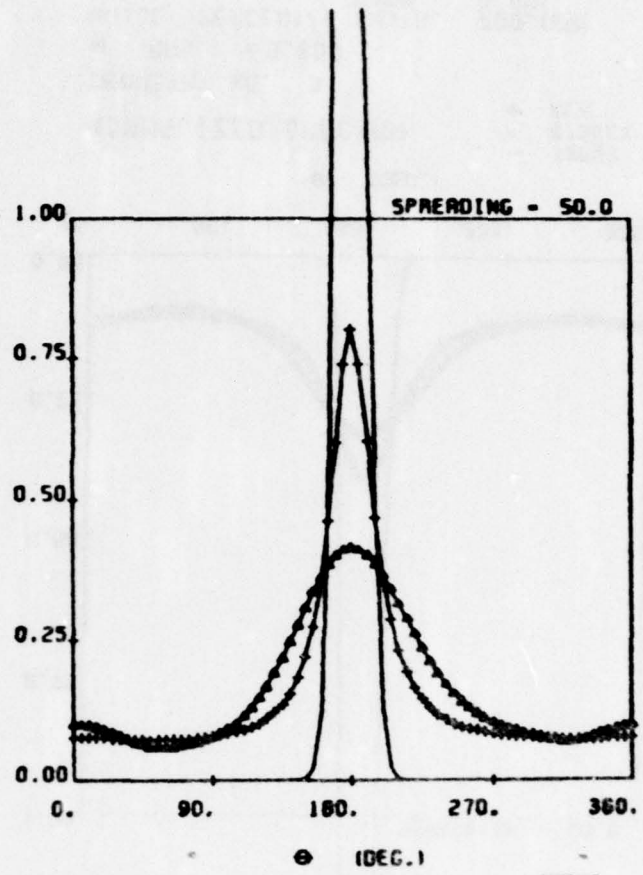

FIGURE VI-10a

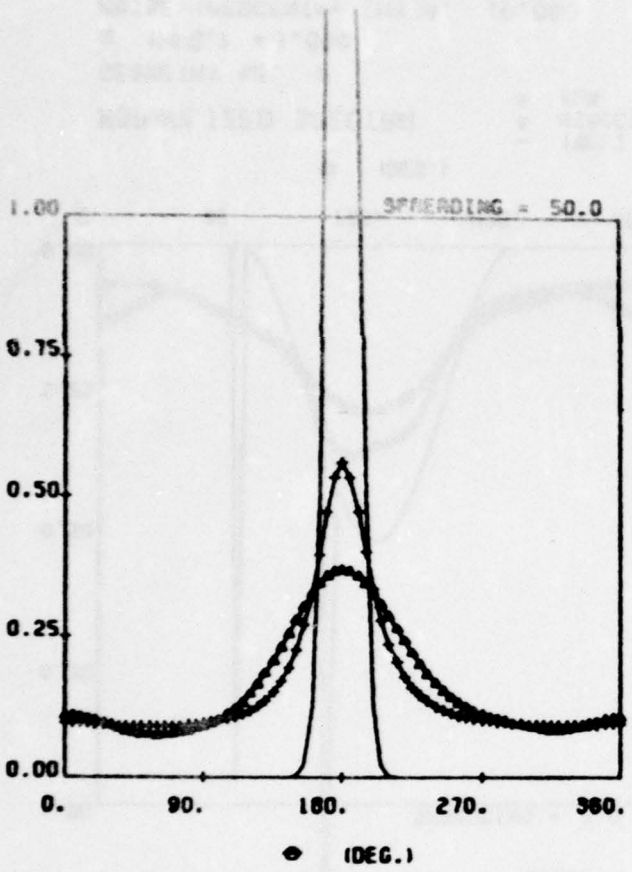

FIGURE VI-10b

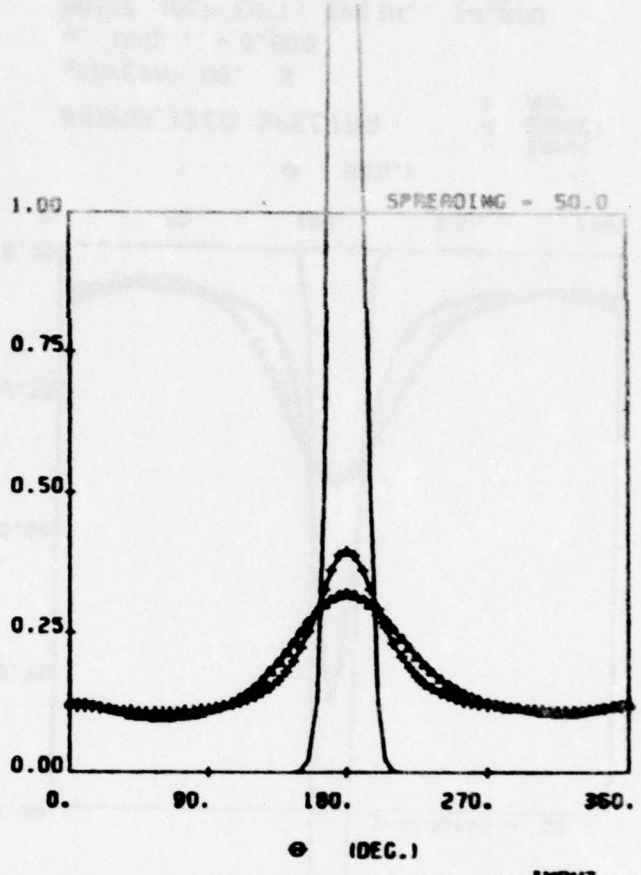

FIGURE VI-10c

into the measuring area, creating a classic "waffle pattern." Assuming the resulting system at f = .4 Hz could be approximated by two plane waves, a noise estimate of the measured data can be obtained by simulation. The array configuration corresponds to Geometry #2 when scaled by a factor of about ten. Figure VI-11 shows the simulated spectral estimate for ten percent instrument noise. Note that the direct method is unable to differentiate between seas separated by ninety degrees! Figure VI-12 shows the MLM spectral estimates of the simulated data for one and ten percent instrument noise with the MLM spectrum of the real data obtained from Figure I-2. The agreement between the measured spectrum and the estimate of the noisy simulation permits an interpretation of the noise level for this particular case. The noise content could be expected to be abnormally high for this example, since the wave amplitudes were exceptionally large, breaking, and confused. Hopefully, ten percent is a practical upper bound for the quantity of noise likely to be encountered under normal operating conditions.

b) Propagating Noise

The only propagating noise that has been modeled is the independent omni-directional distribution discussed in Chapter V. The effect of an omni-directional term is simply to raise the level of the distribution and is handled without apparent difficulty by the MLM analysis.

2. Geometry

a) Array Size

The resolution capabilities of an array increase rapidly as the number of elements N is increased. On the other hand, large arrays are expensive to construct and maintain and should be worth the added cost in resolution. In order to indicate the type of improvement that might be expected for such sparse arrays, a number of other geometries have been investigated. Figures VI-3, VI-13, and VI-14 display the spectral estimates of a three, four, and six element array (Geometries #1, #2, and #3 respectively) in identical wave fields. The signals are all subject to ten per cent instrument noise and $\omega = 0.5$ radians. The improvement in the MLM spectral estimate is evident, particularly for the six element array.

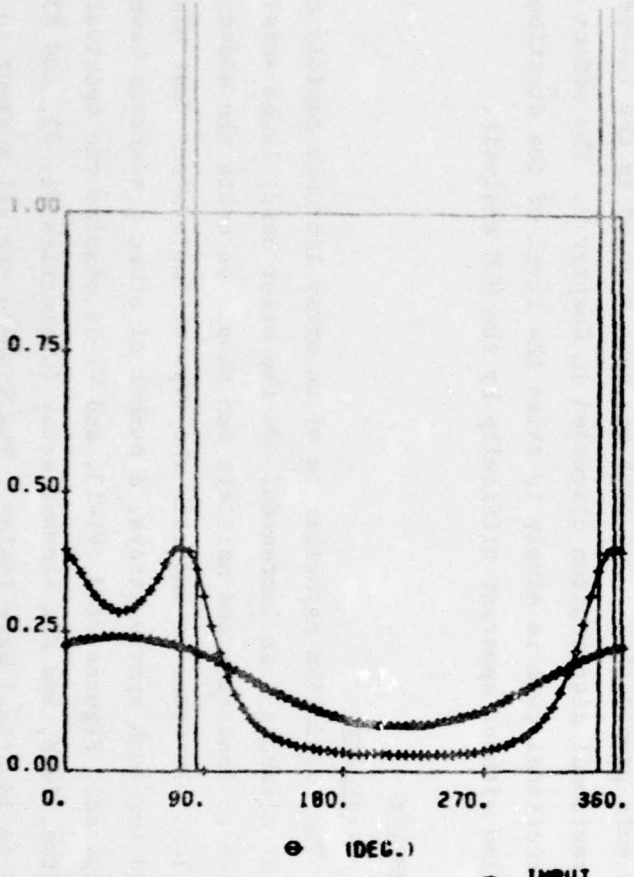

FIGURE VI-11

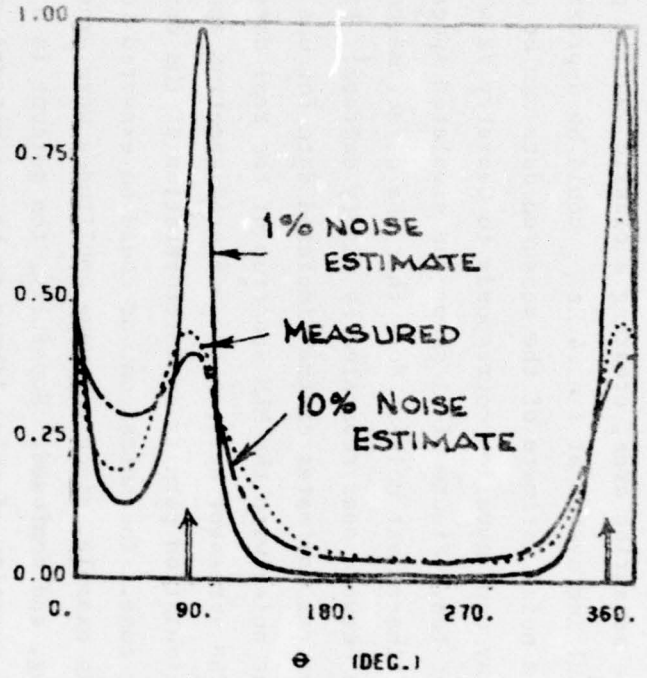

FIGURE VI-12 MLM Spectrum from Measured Data (Fig. I-2) Compared With Simulated Data Spectra for One and Ten Percent Noise Levels

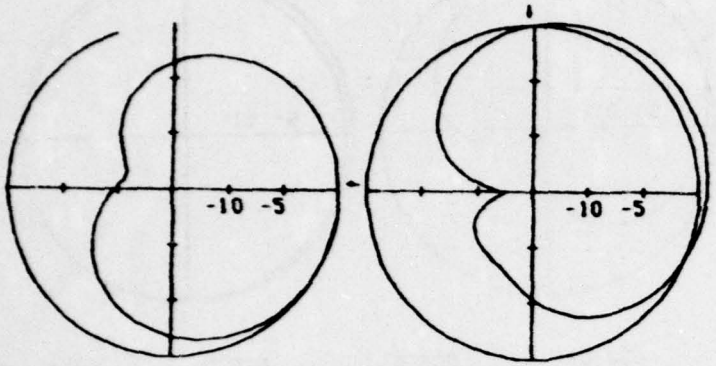

ω (RAD.) 0.500 θ (DEG.) 0.000 ω (RAD.) 0.500 θ (DEG.) 90.000

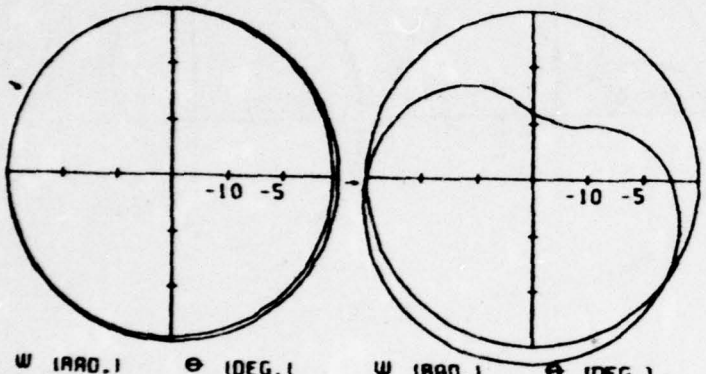

ω (RAD.) 0.500 θ (DEG.) 150.000 ω (RAD.) 0.500 θ (DEG.) 180.000

GEOMETRY NO. 2

BEAM PATTERNS IN DECIBELS (ORIGIN=-150B)

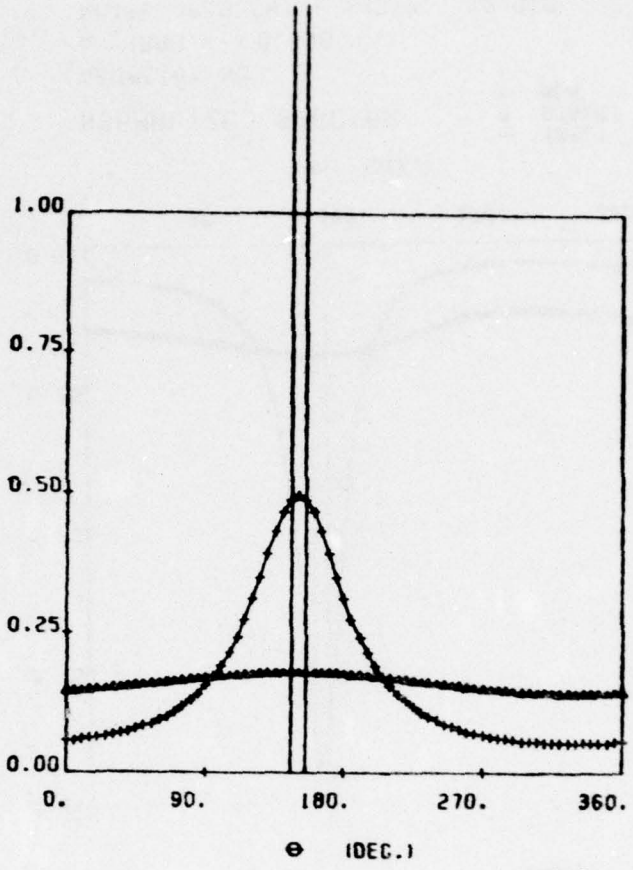

NORMALIZED SPECTRA

– INPUT
▲ DIRECT
+ MLM

GEOMETRY NO. 2

ω (RAD.) = 0.500

NOISE (PERCENT): INSTR. 10.000
PROP. 0.001

FIGURE VI-13

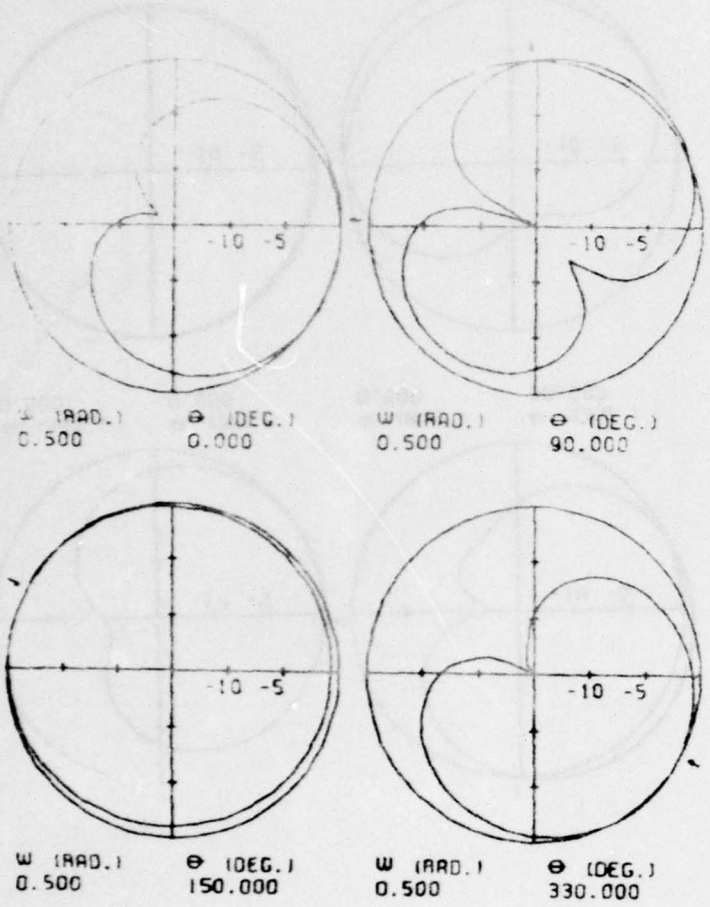

ω (RAD.)	Θ (DEG.)	ω (RAD.)	Θ (DEG.)
0.500	0.000	0.500	90.000
0.500	150.000	0.500	330.000

GEOMETRY NO. 3

BEAM PATTERNS IN DECIBELS (ORIGIN=-15DB)

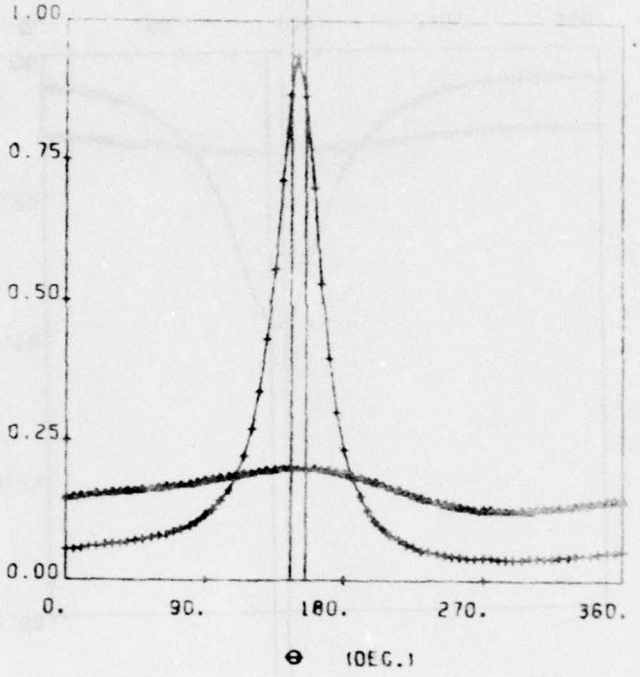

NORMALIZED SPECTRA

– INPUT
▲ DIRECT
+ MLM

GEOMETRY NO. 3

ω (RAD.) = 0.500

NOISE (PERCENT): INSTR. 10.000
PROP. 0.001

FIGURE VI-14

This is primarily due to the increase in N rather than the slightly larger average array size (cf. Appendix A).

Figures VI-7 and VI-15 each have cosine squared distributions with plane wave additions with $\omega = 1.0$ radians and ten percent instrument noise. The six element array shows a distinct improvement over the three element array. There is more shape in the neighborhood of the peak and less omni-directional noise power. The main lobe of the beam pattern of Geometry #3 is narrower and there is far more structure than for Geometry #1.

Vast improvements are possible if the array size is increased to the ten elements of Geometry #5. This configuration is a regular one with the elements spaced evenly on two rings. The array geometry statistics are substantially the same as arrays #3 and #4 and are given in Appendix A. Figures VI-16 and VI-17 are for the same distributed input considered above; $\omega = 1.0$ radians, and the one and ten percent instrument noise levels. The low noise level of Figure VI-16 finally allows the plane waves to become visible whereas they were only hinted at in the six element case. The larger noise level of Figure VI-17 reduces the resolution of the plane waves but is not seriously contaminated by omni-directional energy. The effect of noise is clearly evident in the beam patterns.

b) Element Spacing

The effects of regular vs. irregular array spacing have been investigated by comparing Geometry #3 with Geometry #4. The latter is a six element "double ring" array whereas the former is a somewhat irregularly spaced version that was actually employed in the full scale measurements reported to the NODC (1976). Figure VI-18 is the double ring array with ten percent noise and a wavelength about twice the RMS gage pair distance. There is a fair amount of structure evident in the beam pattern and in the estimated MLM distribution. The corresponding case for the irregular geometry is shown in Figure VI-15. There is a slight decrease in the amount of aliasing at the expense of some resolution. These differences are evident in the variations of the beam patterns. In general, a regularly spaced array will have a beam pattern with a narrow main lobe but rather pronounced side lobes. If the array spacing is perturbed so that it is no

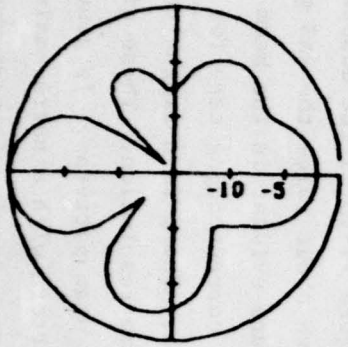

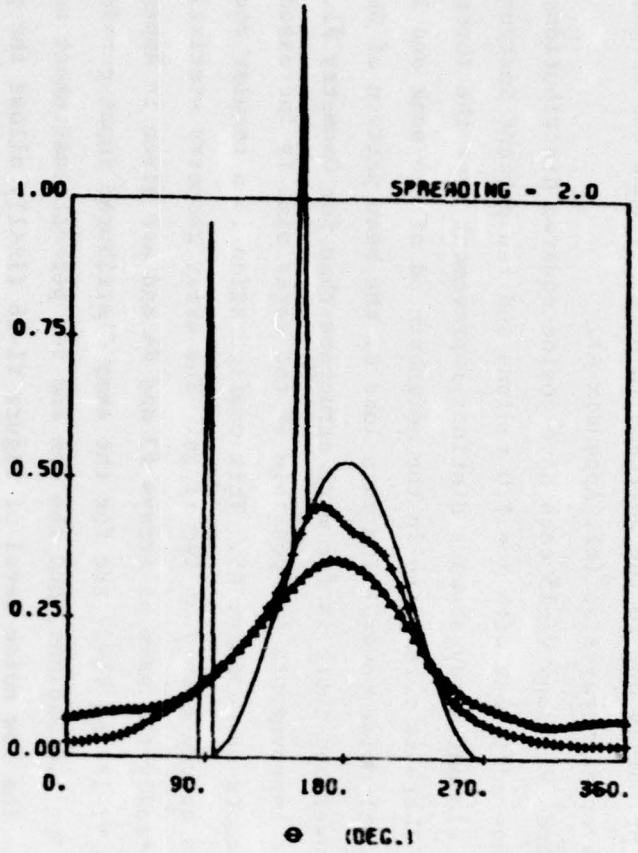

GEOMETRY NO. 3

BEAM PATTERNS IN DECIBELS (ORIGIN=-150B)

FIGURE VI-15

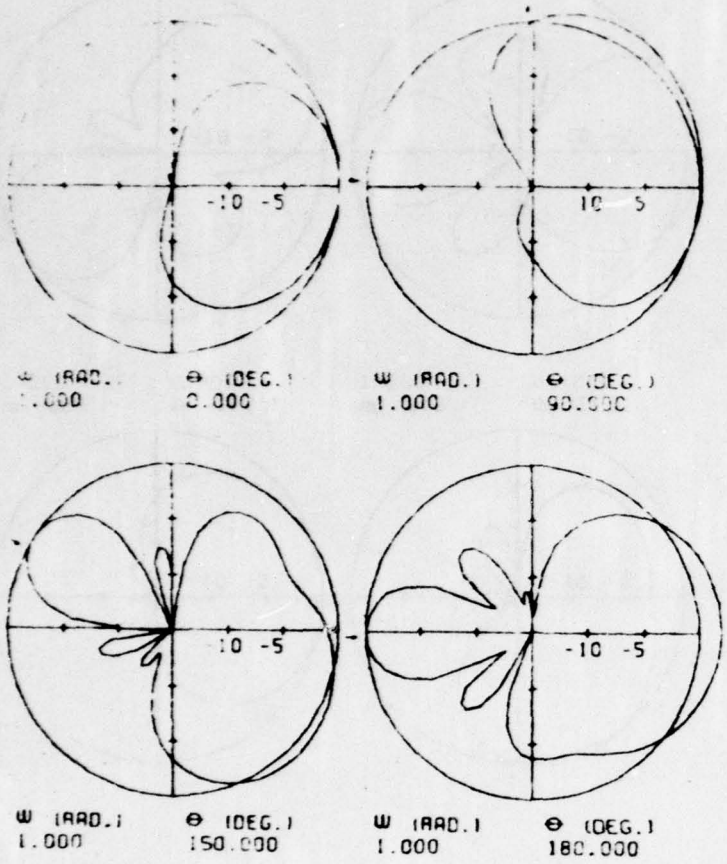

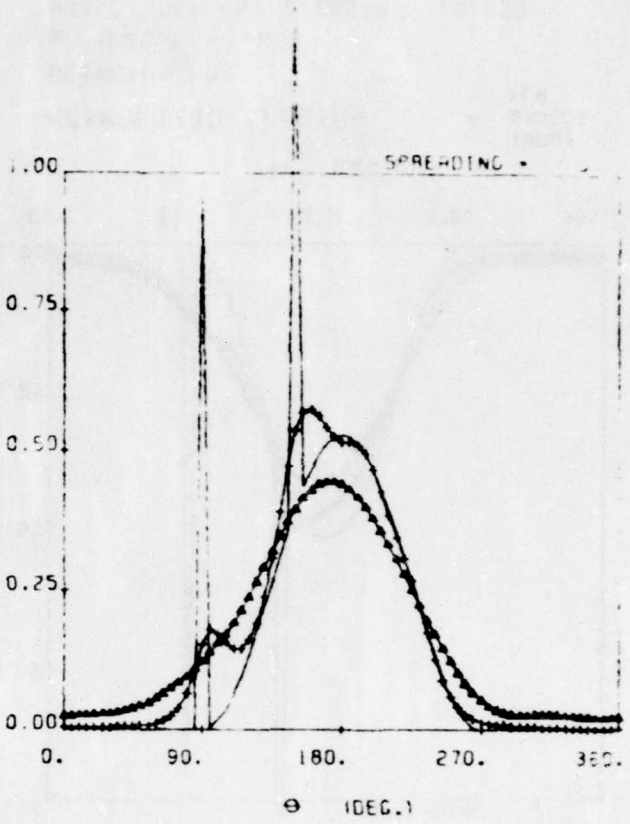

FIGURE VI-16

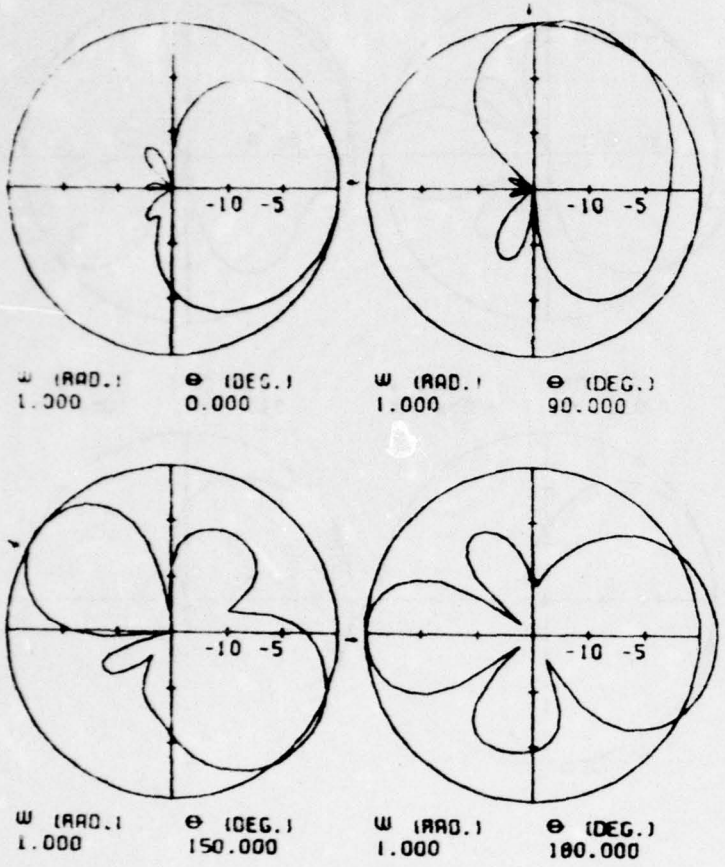

GEOMETRY NO. 5

BEAM PATTERNS IN DECIBELS (ORIGIN=-15DB)

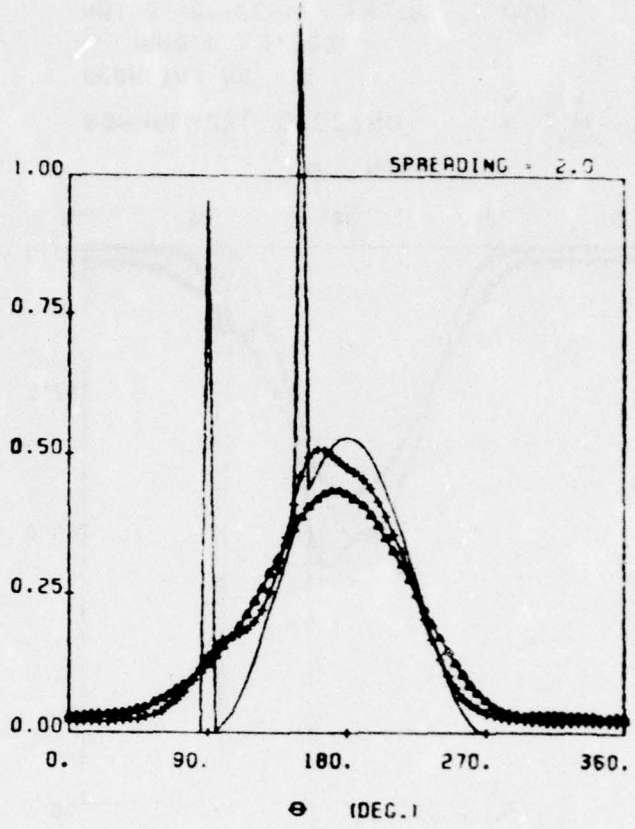

NORMALIZED SPECTRA

GEOMETRY NO. 5

ω (RAD.) = 1.000

NOISE (PERCENT): INSTR. 10.000
PROP. 0.001

FIGURE VI-17

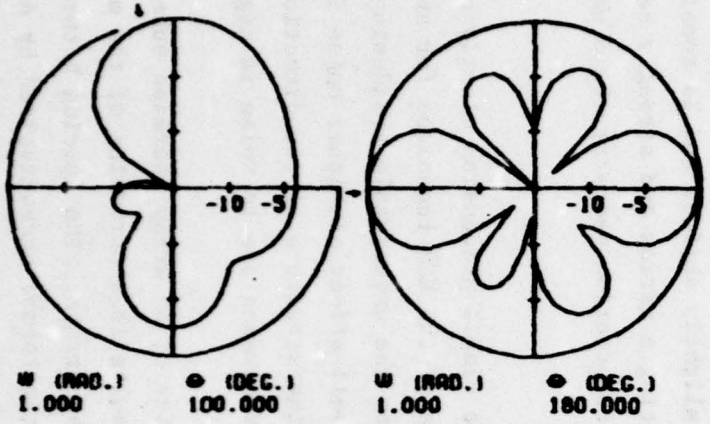

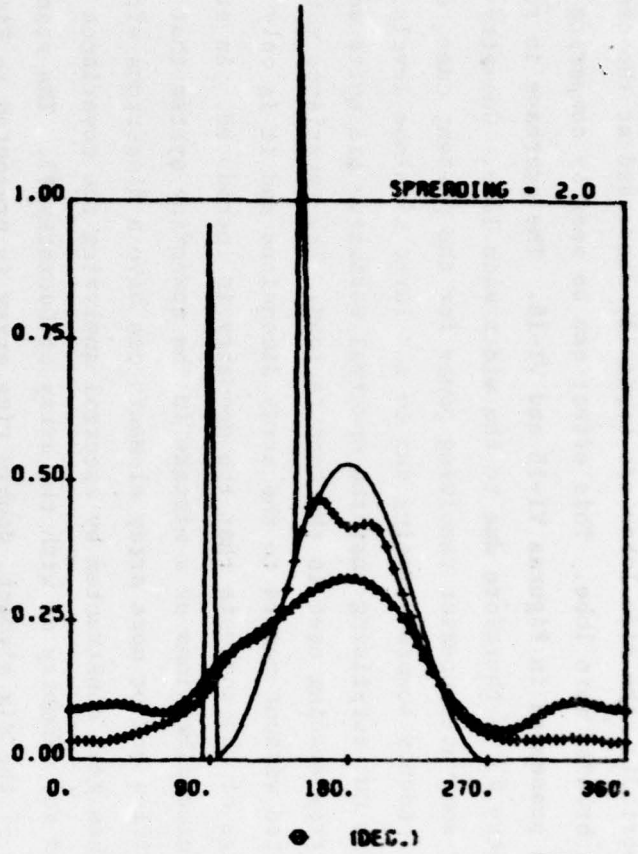

GEOMETRY NO. 4

BEAM PATTERNS IN DECIBELS (ORIGIN=-150B)

FIGURE VI-18

longer periodic, the side lobes are typically decreased at the expense of a somewhat broader main lobe. This effect can be seen by comparing the patterns presented in Figures VI-15 and VI-18. The decrease in resolution of Geometry #3 is therefore due to the wider main lobe. Geometry #4, while having a somewhat superior resolving power for the present case, does exhibit a tendency toward aliasing due to the large sidelobe levels.

It is not surprising that the spectral estimates are quite sensitive to the array spacing used in the computations. The covariance matrix is constructed without regard to the array dimensions and it is only in the last stage of the analysis that the geometry is introduced. An error in the measured dimensions or a mistake in the numbering system that in effect shuffles one or more array elements can have a disastrous effect. An example has been constructed by spectral analyzing the covariance matrix generated for Geometry #4 with the array of Geometry #3. The standard analysis of the six element, double ring array is presented in Figure VI-18. If this same covariance matrix is analyzed with the irregular spacing of Geometry #3 the spectral estimate is radically altered as shown by Figure VI-19. The spectral peak is slightly shifted and is considerably narrower. If the investigator was expecting a narrow and strongly centered distribution, such an error in the computation geometry could easily go undetected.

3. Summary

Noise contamination of the signal processing clearly has adverse effects on the resolution capabilities of the MLM technique for any array configuration. This is manifested by the undesirable broadening of the main lobe of the beam pattern. The overall effect of higher noise levels on the MLM is to blur and disperse the fine structure of the directional spectrum. The fractional decrease in performance due to noise is highest for denser arrays.

The resolution capabilities of an array increase substantially with the number of elements and results in a narrowing of the main lobe. This is particularly true for sparse arrays. The spacing between elements may be regular or irregular with the former characterized by a narrower main lobe but somewhat higher side lobes than the latter.

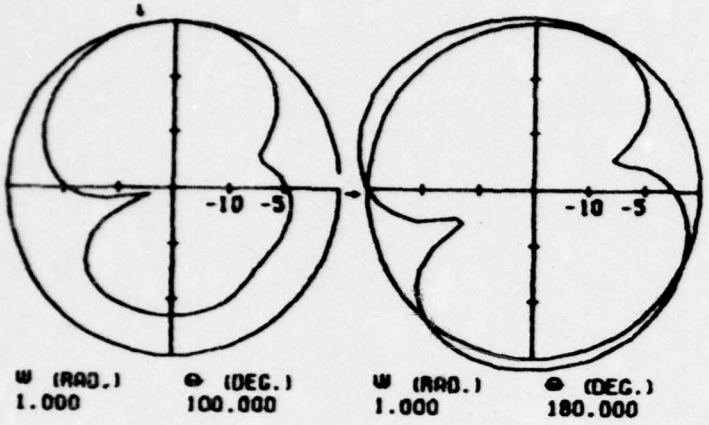

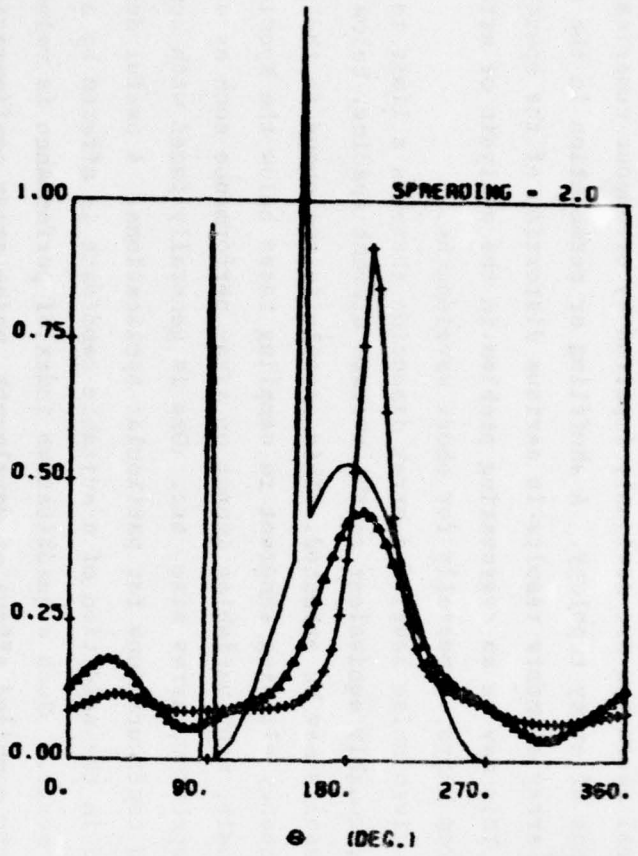

GEOMETRY NO. 3

BEAM PATTERNS IN DECIBELS (ORIGIN=-150B)

FIGURE VI-19

Spectral estimates are seriously impaired by erroneous numerical perturbations of array topology. A shuffling or permutation in the ordering of the array elements results in serious distortion of the spectral estimate. This may be an aggravating problem in the analysis of array data obtained from buoys, especially for short wavelengths.

For a given noise level and array dimension there is a limit to the wavelength, roughly equivalent to the average element spacing, below which spurious results may be expected. This anomaly is analogous to the problem of frequency aliasing inherent to sampling rates below the Nyquist rate.

Obviously, many variables impact on array performance such as a specific input spectrum, array size, etc. One is generally faced with competing designs and configurations for particular applications. A useful design tool to aid in the selection of a suitable candidate is affored by a "figure of merit." Such a quantitative index of performance is valuable in assessing the combined effect of wavelength, noise array configuration and directional distribution of input energy. A convenient figure of merit will be developed in Chapter VII.

VII. FIGURES OF MERIT

The overall performance of the array is, naturally, a function of the intrinsic geometry and sensor characteristics as well as the particulars of the ambient wave field. Selecting the most suitable array geometry among a variety of configurations is a difficult task indeed, due in part to the nonlinear nature of the MLM. While no optimization technique is currently available for array selection (it may not even be worth the effort!) a simple index or measure, i.e., a figure of merit, is necessary to differentiate between candidates.

Initially, the number of elements as well as their spacing are variables which must be chosen in a manner consistent with the expected wave field. Obviously, the wave spectrum is not known a priori (except perhaps in a gross sense) and we are forced to choose one or more design (directional) wave elevation spectra and assess, via analysis and/or simulation, the array performance. Once the designer has chosen his design spectra, he is faced with the problem of rating the performance of the array candidates. This is most easily accomplished by simulation where the (simulated) "estimated" spectrum is usually compared with the input or design spectrum over all directions and frequencies. However, it seems apparent that a quantitative performance index or a "figure of merit" is desirable in that it is a more efficient scheme than visual inspection of reams of print-out. The figure of merit must be a consistent estimate of performance and inevitably must reflect the average resolution of the array for a given design spectrum. To this end, consider the frequency variable (ω_o) fixed for this discussion. Since we are concerned here only with the spatial spreading, let $B[\theta;\omega/\Theta_o\omega_o]$ represent the natural beam pattern of the array as defined in Chapter IV. Let $F(\theta)$ represent the spreading function which has been normalized such that

$$\int_0^{2\pi} F(\theta)\, d\theta = 1.0 \quad .$$

In order to fix ideas, consider the natural beam pattern. In this case, $B[\theta; \omega/\Omega_o; \omega_o]$ is ideally relatively narrow or peaked about the look angle $\theta = \theta_o$ and the spectral estimate (eq. 7.1) may be written;

$$E\{\hat{S}(\theta_o, \omega_o)\} \cong S(\omega_o) F(\theta_o) \int_0^{2\pi} B[\theta; \omega | \theta_o; \omega_o] \, d\theta . \tag{7.1}$$

Furthermore, for this natural beam pattern, the integral

$$\int_{-\pi}^{\pi} B[\theta; \omega | \theta_o; \omega_o] \, d\theta \tag{7.2}$$

may be interpreted as the effective beamwidth of the array at $\theta = \theta_o$. In practice, however, MLM beam patterns are not peaked enough and hence do not always satisfy the approximation of Eq. (7.1) for all θ_o. A figure of merit should be a measure of the divergence from good resolutions, hence define the quantity $I(\theta_o; \omega_o)$:

$$I(\theta_o; \omega_o) = \int_{-\pi}^{\pi} F(\theta) B[\theta; \omega | \theta_o; \omega_o] \, d\theta . \tag{7.3}$$

Some consideration of Eq. (7.3) leads to the conclusion that the narrower the effective beamwidth about $\theta = \theta_o$ the smaller the value of $I(\theta_o; \omega_o)$. Now the fraction of energy incident in a neighborhood θ_o of a given look angle $\theta = \theta_o$ is $I(\theta_o; \omega_o)$. It follows that a "weighted" measure of array performance, call it $P(\theta_o; \omega_o)$, is:

$$P(\theta_o; \omega_o) = F(\theta_o) / I(\theta_o; \omega_o) \tag{7.4}$$

and thus the performance averaged over all look angles $0 \le \theta_o \le 2\pi$ is:

$$\bar{P}(\omega_o) = \frac{1}{2\pi} \int_{-\pi}^{\pi} P(\theta_o; \omega_o) \, d\theta_o . \tag{7.5}$$

We may define an array gain by taking the ratio (in db's) of $\bar{P}(\omega_o)$ of the given array to that of a single element which is inherently omni-directional. For a single element $B[\theta;\omega|\theta_o;\omega_o] = 1$, all (θ, θ_o), and (ω,ω_o) from Eqs. (7.3) through (7.5), it follows that:

$$\left[\bar{P}(\omega_o)\right]_{\substack{\text{single}\\ \text{element}}} = \frac{1}{2\pi} . \tag{7.6}$$

Therefore, the array gain is simply $2\pi\,\bar{P}(\omega_o)$.

From Eq. (7.6) it follows, for example, that the array gain of a single element is 0 DB's while that of an array with say twice the average resolution is 3 DBs. The array gain is a measure of the <u>average</u> performance (i.e., averaged over all look angles $-\pi \leq \theta_o < \pi$).

We choose, therefore, in the discussions to follow, to define the figure of merit (denoted F.O.M.) as the array gain in decibels, i.e.

$$\text{F.O.M.} = 10 \log_{10}(2\pi\bar{P}(\omega_o)). \tag{7.7}$$

Though the ability of a given array to resolve directional spectral features at various wavelengths (or frequencies) is highly geometry dependent, resolution trends should be the same regardless of the particular algorithm (direct or adaptive) implemented. In the case of the natural beam pattern, for example, expression (4.8) exhibited the inverse relationship between the half-power beamwidth and the root-mean-square distance of the sensor elements from the arrays geo-center.

Figure VII-1 shows a plot of the F.O.M. vs. normalized wavelength for four arrays. The wavelength has been scaled by the average interprobe distance of each individual array. The directional spreading of the incident wave field was modeled as a mixture of two delta functions and a cosine-squared function. It was felt that this directional distribution was a reasonable combination with which to test the performance of the MLM algorithm in conjunction with the various array geometries. As expected, there is a notable improvement in performance as the number of sensors increases, especially in that region where the wavelength is on

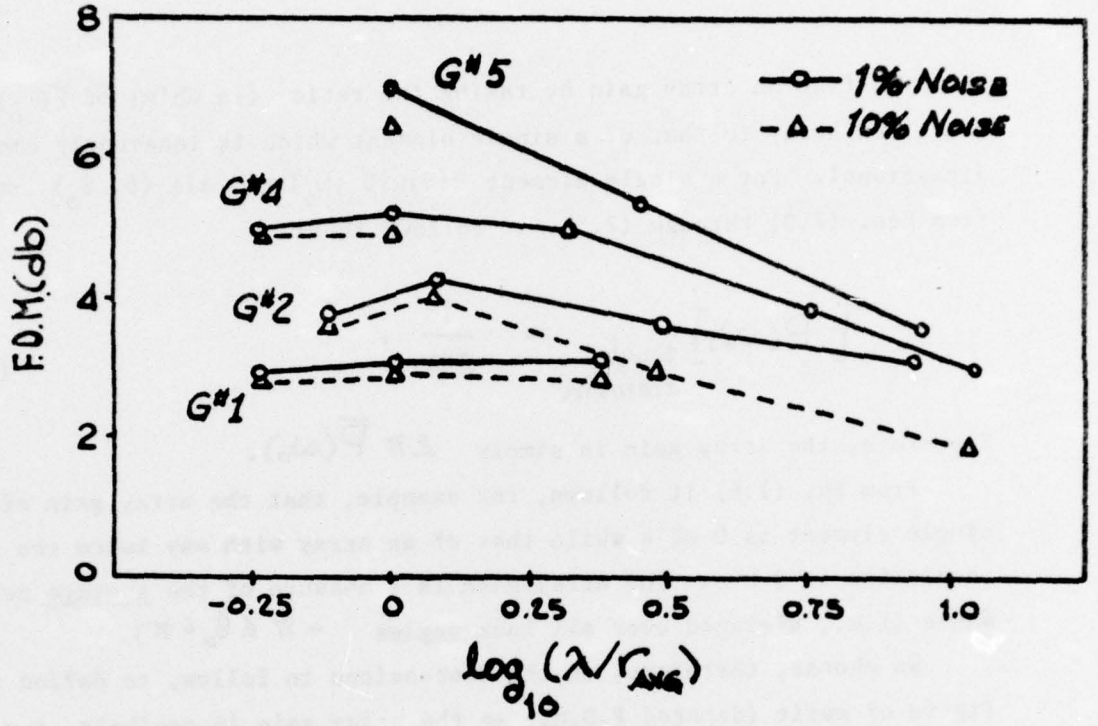

FIGURE VII-1

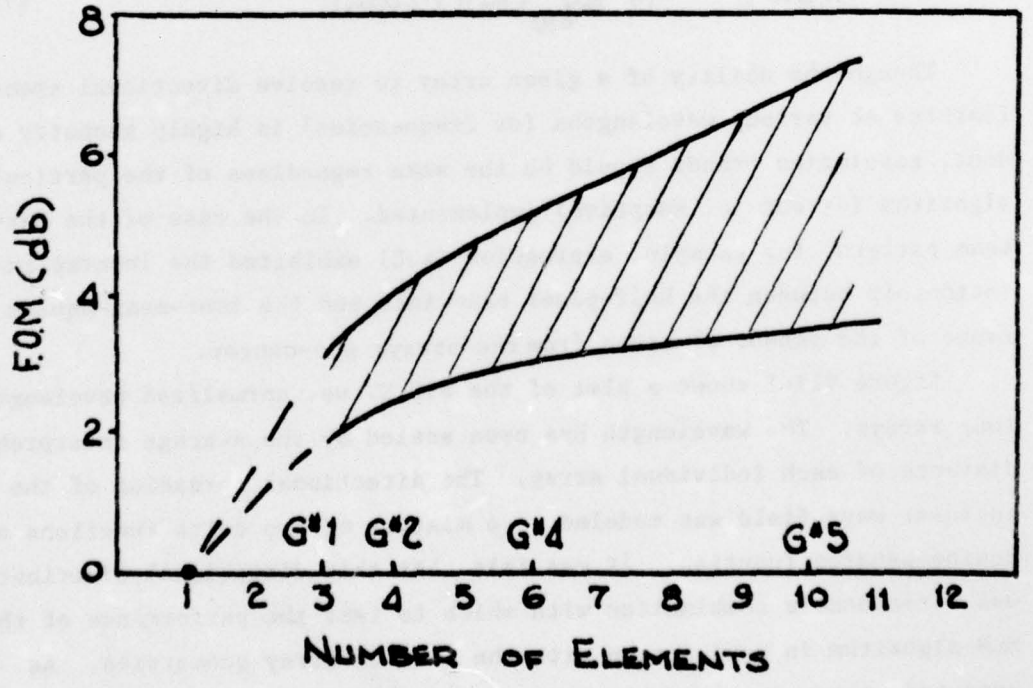

FIGURE VII-2 Max/Min Performance (1% Noise)

the order of the average interprobe distance. In particular, when the wavelength is about equal to the interprobe distance the rate of increase of the F.O.M. is roughly asymptotic to .45 db's per sensor. As the wavelength grows large compared with the interprobe distance the performance of all the arrays diminishes to 0 db since the array, regardless of the number of sensors, is in the limit effectively reduced to a single probe (i.e., no resolution capability). As is apparent in Figure VII-2, the rate of increase in performance per sensor dwindles for larger normalized wavelengths.

Instrument noise, of course, degrades performance particularly at the longer wavelengths. From the dashed lines on Figure VII-1 which represents individual array performance with ten percent noise it appears that the relative degree of degradation is greatest for the densest arrays. In other words, the denser arrays have "more to lose" in terms of resolution capability and it appears that increasing the number of noisy probes is no guarantee of greater resolution.

VIII. SUMMARY AND ARRAY DESIGN

1. Summary

The directional or angular spreading of ocean wave energy demands spectral estimation techniques of sufficient resolution. Higher resolution can usually be achieved by increasing the size of the array of wave sensors though usually at great cost. An alternative to greater array size is the nonlinear MLM estimation algorithm. In Chapter III it was shown how 1) directional spectra were naturally associated with spatial Fourier transforms, and 2) the formulation of the direct and MLM spectral were computed in terms of the covariance matrix. In Chapter IV it was demonstrated how the natural or effective beam pattern related the true spectrum to the estimated spectrum in the direct and MLM procedures. The interpretation of the beam pattern and spectral spreading plots were discussed in detail. Chapter V presented the details of the synthesis of the directional spectrum and covariance matrix used in the simulations. In Chapter VI, the effects of noise, wavelength, number of elements and spacing on array performance and resolution were analyzed using the simulation of Chapter V. In particular:

i) Noise contamination of the signal processing has adverse effects on the resolution capabilities of the MLM technique for all array configurations,

ii) The resolution potential of sparse arrays increased dramatically with the number of elements but is not highly dependent on the element spacing within the array itself.

In Chapter VII, a figure of merit was derived and applied to the example considered earlier. A suitable figure of merit (FOM) is instrumental in the selection of an appropriate array configuration from competing designs.

2. Array Design

It is not yet possible to construct design charts for the selection of array sizes and geometry on the basis of the analysis presented above. A major unresolved question is the amount of noise present in the signal.

Estimates of the instrument noise can be made once the sensor type has been selected. Estimates of the amount of ambient field noise, both propagating and non-propagating, are more difficult to obtain. It will therefore be necessary to assume conservative values for the amount of noise modeled in the simulation.

It was shown in Chapter VI that the MLM spectral estimate approaches the direct estimate as the noise level becomes large. This allows one to use the results of the natural beam pattern analysis in order to determine a lower bound on the resolution capabilities of a given array configuration. If such a worst case design is geometrically and economically feasible, then the actual MLM resolution will presumably be considerably better. If the conservative approach does not yeld a practical array, more accurate noise estimates and additional simulation should be attempted.

A simplified approach to the preliminary design or selection of an array for a specific application is offered below:

1) Estimate the range of wavelengths of interest. A sample point spectrum will indicate the frequency range containing significant ambient wave energy. The particular application of the data will generally suggest a maximum and minimum wavelength bounding the range of major interest. For example, if the problem is to predict the motions of a ship in a seaway, the high frequency limit might be derived from a consideration of the roll response. Waves on the order of the ship's beam or smaller, for example, will have little effect. The low frequency limit should definitely be below the region of maximum motion response and hopefully include the most energetic portions of the wave spectrum.
2) The next step is the estimate of the amount of resolution considered to be essential. A convenient approach is to select a maximum acceptable width of the main lobe of the beam pattern, $2(\theta_{1/2})$. This is indicative of the amount the true spectrum will be smeared out in the process of estimation. An upper limit of the RMS array radius

can be obtained from the natural beam pattern analysis, Eq. (4.8) as

$$r_{RMS} \simeq \frac{18.2\,\lambda}{(\theta_{1/2})}$$

where $(\theta_{1/2})$ is the half-power beam width divided by two. The MLM beam width is certain to be narrower, hence better resolving, than the direct analysis.

3) The short wavelength limit can be used to establish an upper limit for the gage pair distances. In order to avoid serious spatial aliasing, the majority of the r_{ij}'s should be less than the minimum wavelength for which a directional spreading estimate is desired.

4) The most important question concerns the number of elements or sensors that will be necessary. The relative improvement in resolution for an increase in N is shown in Figure VII-2. One should bear in mind that the rate of improvement in resolution decreases as the amount of sensor noise increases. Probably the best approach would be to conduct a sensitivity analysis for various amounts of spreading in the spectral estimate. This, combined with a reasonable noise estimate and the MLM simulation, should provide a sound estimate for the minimum number of elements.

5) Array shape is likely to be somewhat less important than the above estimates of r_{RMS}, r_{ijmax}, and N. Local structure to support the array and questions of safety of the sensors usually dictate to some extent the range of geometries available. The above analysis has always assumed that the waves could come from any direction or that the orientation

of the array could not be controlled. If this is not the case, array geometries that are not essentially equally distributed are conceivable.

In conclusion, the MLM offers greater directional resolution potential than any of the direct methods of spectral analysis. Signal noise is inherent in all measuring situations. The quality of the MLM spectral estimate can be seriously impaired by such noise contamination. Therefore, it is essential that accurate estimates of the intrinsic noise levels in the measuring system be obtained in order to insure adequate resolution with the smallest possible array.

REFERENCES

1. Baggeroer, A., 1976: Lecture Notes, Department of Ocean Engineering, M.I.T.

2. Barber, N.F., 1961: "The directional resolving power of an array of wave detectors", Proc. Conf. Ocean Wave Spectra, Easton, Maryland, Prentice-Hall, Inc., Englewood Cliffs, New Jersey, 137-150.

3. Barnett, T.P., 1969: "Wind waves in shallow water", Final Report, Westinghouse Ocean Research Laboratory, San Diego, California, June.

4. Bendat, J.S. and A.G. Piersol, 1971: Random Data: Analysis and Measurement Procedures, Wiley-International.

5. Bennett, C.M., E.P. Pittman, and G.B. Austin, 1964: "A data processing system for multiple time series analysis of ocean wave induced bottom pressure fluctuations," Proc., 1st U.S. Navy Symposium on Military Oceanography, June.

6. Blackman, R.B. and J.W. Tukey, 1958: The Measurement of Power Spectra from the Point of View of Communications Engineering, Dover Publications, Inc., New York.

7. Borgman, L.E. and N.N. Panicker, 1970: "Design study for a suggested wave gage array off Pt. Mugu, California", Technical Report HEL-14, Hydraulic Eng. Lab., University of California - Berkeley, January.

8. Capon, J., 1969: "High-resolution frequency-wavenumber spectrum analysis", Proc. of the IEEE, Vol. 57, No. 8, August.

9. Capon, J., R.J. Greenfield, and R.J. Kolker, 1967: "Multidimensional maximum-likelihood processing of a large aperture seismic array", Proceedings of the IEEE, Vol. 55, No. 2, February.

10. Chou, Oakley, Paulling, Van Slyke, Wood, Zink, 1974: "Ship motions and capsizing in astern seas", Final Report for Department of Transportation; U.S. Coast Guard, Department No. CG-D-103-75, December.

11. Cote, L.J., et.al., 1960: "The directional spectrum of a wind generated sea as determined from data obtained by the Stereo Wave Observation Project", Meteor. Paper, Vol. 2, No. 6, N.Y.U. Press, New York, June.

12. Draper, L. and B.C.H. Fortnum, 1974: "Wave recording instruments for civil engineering use", Institute of Oceanographic Sciences, Wormley, Great Britain, July.

13. Guthart, H., U.S. Krishnan, and N.A. Peppers, 1975: "Measurement of surface-wave statistics", J. Hydronautics, Vol. 9, No. 4, October.

14. Haddara, et.al., 1972: "Capsizing experiments with a model of a fast cargo liner in San Francisco Bay", Department of Naval Architecture, University of California - Berkeley. Prepared for the U.S. Coast Guard, Office of Research and Development, Project 723411, January.

15. Hasselmann, K., D.B. Ross, P. Miller, and W. Sell, 1976: "A parametric wave prediction model", J. of Physical Oceanography, Vol. 6, March, p. 200-228.

16. Hasselmann, et.al., "Measurements of wind-wave growth and swell decay during the North Sea Wave Project (JONSWAP)", Report by the Deutsches Hydrographiches Institut, Hamburg, 1973.

17. Jenkins, G.M. and D.G. Watts, 1969: Spectral Analysis and Its Applications, San Francisco, Holden-Day, 525 pp.

18. Lacoss, R.T., 1971: "Data adaptive spectral analysis methods", Geophysics, Vol. 36, pp. 661-675, No. 4, August.

19. McDonough, R.N., 1972: "Degraded performance of nonlinear array processors in the presence of data modeling errors", J. of the Acoustical Society of America, Vol. 51, No. 4 (Part 1).

20. Mollo-Christensen, E. and P. Koziol, 1972: "Underway and scanning measurement of air-sea surface layer properties", MIT Department of Meteorology, September.

21. NODC, 1976: "Wave data submitted to the National Oceanographic Data Center by Deep Oil Technology, Inc.", February 1976. National Oceanographic Data Center, Records Section, Rockville, Maryland 20852.

22. Panicker, N.N., 1974: "Review of techniques for directional wave spectra", Int. Symp. on Ocean Wave Measurement and Analysis, New Orleans, September, A.S.C.E., Vol. 1, p. 669.

23. Pierson, W.J., 1976: "The theory and applications of ocean wave measuring systems at a below the sea surface, on the land, from aircraft, and from spacecraft," NASA CR-2646, January.

24. Otnes, R.K. and L. Enochson, 1972: Digital Time Series Analysis, John Wiley and Sons, Chapter 7.

APPENDIX A

Array Geometries

This Appendix includes representative small array geometries. Figure A-1 shows the array configurations to the same scale. The angle θ is measured counter-clockwise from the x-axis.

Table A.1 lists the coordinates (ft.) of the array elements used in the simulation analysis. Table A.2 gives a number of array geometry statistics for the arrays of Table A.1.

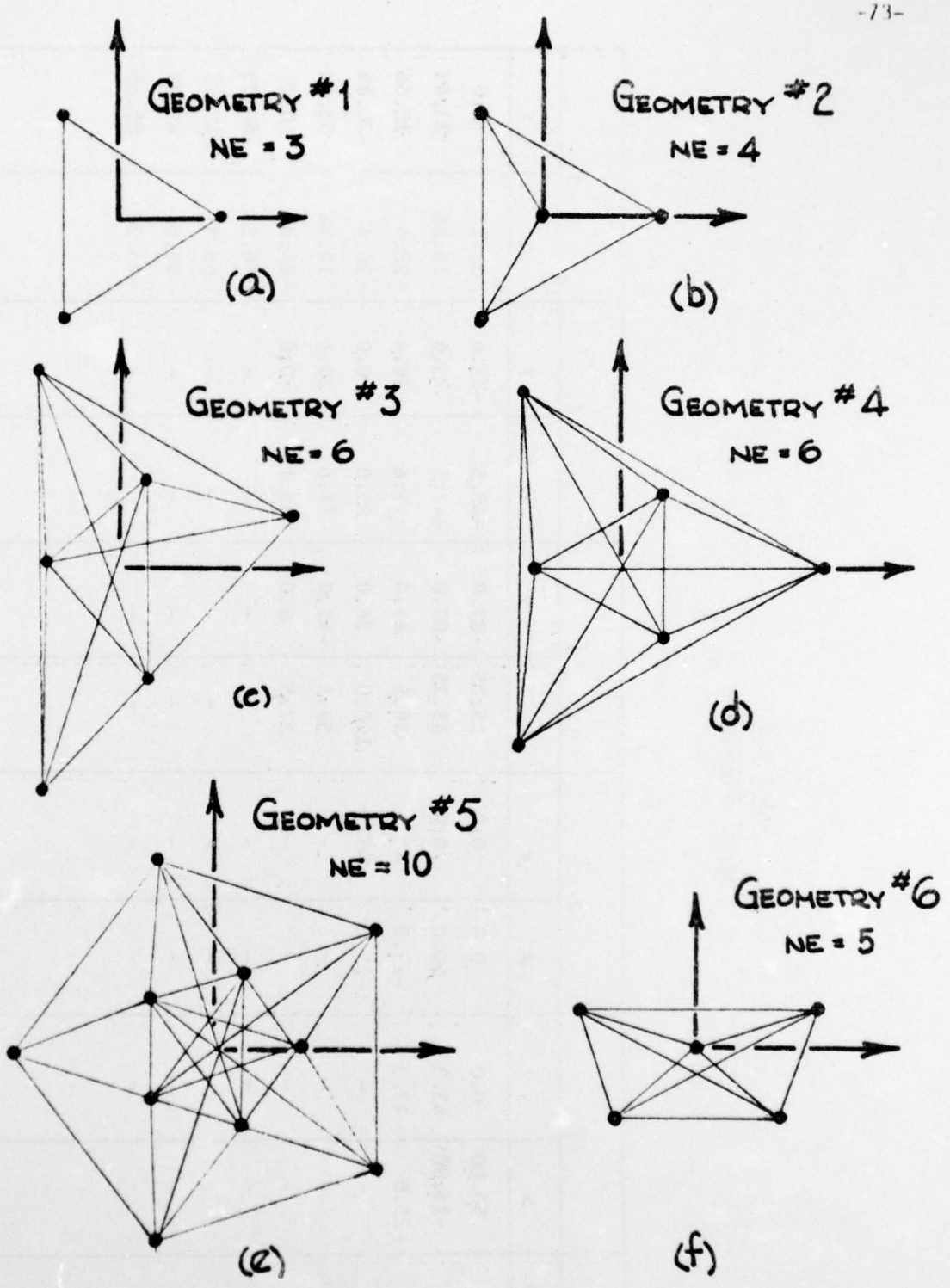

FIGURE A-1 Array Geometries

TABLE A.1

ARRAY GEOMETRIES

Geometry Number	1		2		3		4		5	
ELEMENT	x	y	x	y	x	y	x	y	x	y
1	50.00	0.0	0.0	0.0	15.25	-87.0	-42.5	-73.6	35.15	0.0
2	-25.00	43.3	50.0	0.0	15.25	87.0	-42.5	73.6	10.86	33.43
3	-25.0	-43.3	-25.0	43.3	58.5	41.0	17.6	30.4	-28.4	20.66
4	-	-	-25.0	-43.3	120.0	26.0	85.0	0.0	-28.4	-20.66
5	-	-	-	-	58.5	-41.0	-17.6	30.4	10.86	-33.33
6	-	-	-	-	17.5	8.0	-35.1	0.0	-85.05	0.0
7	-	-	-	-	-	-	-	-	-26.28	-80.89
8	-	-	-	-	-	-	-	-	68.81	-49.99
9	-	-	-	-	-	-	-	-	68.81	49.99
10	-	-	-	-	-	-	-	-	-26.28	80.89

TABLE A.2

ARRAY STATISTICS IN FEET

GEOMETRY NUMBER	NUMBER OF ELEMENTS	RADIUS*			
		MIN.	AVG.	RMS.	MAX.
1	3	50.0	50.0	50.0	50.0
2	4	0.0	37.5	43.3	50.0
3	6	30.1	62.7	67.7	98.1
4	6	23.4	56.9	64.0	91.5
5	10	35.1	60.1	65.1	85.0

GEOMETRY NUMBER	NUMBER OF ELEMENTS	GAGE PAIR DISTANCES**			
		MIN.	AVG.	RMS	MAX.
1	3	86.6	86.6	86.6	86.6
2	4	50.0	68.3	70.7	86.6
3	6	52.6	98.4	104.9	174.0
4	6	35.1	91.6	99.2	147.3
5	10	41.3	90.4	97.0	161.0

*Radius measured from the geometric mean.

**Gage pair statistics computed for the independent gage pairs, i.e. for $r_y = |\underline{x}_i - \underline{x}_j|$, $j \neq i$.

APPENDIX B

Directional Spreading Models

The following spreading functions have been used as examples in the simulation described in Chapter V, Section 1.

Omnidirectional Spectrum

This spectrum represents a ring of random plane waves propagating uniformly in all directions. The spreading function is flat over the 2π radians of azimuth, i.e., $F(\theta) = 1/2\pi$, and the Fourier coefficients from Eq. (5.6) are:

$$a_n = \begin{cases} 1/2\pi & n=0 \\ 0 & n\neq 0 \end{cases} \tag{B.1}$$

The covariance function becomes simply,

$$C(\omega,\xi) = S(\omega) J_o(kr)/2\pi \tag{B.2}$$

This function may be used to model the phenomenon of propagating noise as well as ocean spectra.

Raised Cosine Directional Spectrum

This spectral spreading function is given by

$$F(\theta) = c \cdot \cos^p(\theta-\theta_o) \qquad |\theta-\theta_o| < \frac{\pi}{2} \tag{B.3}$$

where p is arbitrary and "c" is a normalization constant such that $a_o = 1/2\pi$. This spectrum represents energy propagating to a point from a half-space about the ray $\theta = \theta_o$. The higher the value of p the more heavily concentrated is the energy about $\theta = \theta_o$. It's expansion coefficients are:

$$a_n = \frac{e^{jn\theta_o} \int_0^{\pi/2} \cos(n\theta)\cos^p(\theta)\,d\theta}{2\pi \int_0^{\pi/2} \cos^p(\theta)\,d\theta}, \quad (n=0,\pm1,\pm2,\ldots). \tag{B.4}$$

A typical example of the raised cosine spectrum is the "cosine squared" spreading function (p=2 in Eq. B.4) centered about $\theta = \theta_o = 0$. In this special case,

$$a_n = \frac{4\sin(\pi n/2)}{\pi^2 n(4-n^2)}, \quad (n=0,\pm1,\pm2,\ldots). \tag{B.5}$$

In the digital computations, it was found expedient to integrate Eq. (5.3) numerically for each p of interest rather than compute the a_n coefficients and then evaluate all the Bessel functions as dictated by Eq. (5.7).

Delta Function Directional Spectrum

This spectrum represents energy propagating in a single direction, say along all lines parallel to the ray $\theta = \theta_o$. Mathematically, the spreading function is represented by:

$$F(\theta) = \delta(\theta-\theta_o) \tag{B.6}$$

and substituting into Eq. (5.3) yields directly

$$C(\omega,\Sigma) = \frac{1}{2\pi} e^{-jkr\cos(\theta_o-\varphi)}. \tag{B.7}$$

This is easily extended to an arbitrary number of spikes, i.e.,

$$F(\theta) = \frac{1}{B}\sum_{m=1}^{M} b_m\,\delta(\theta-\theta_m) \tag{B.8}$$

where $B = \sum_{m=1}^{M} b_m$. It follows that the covariance function for a set of M

spikes is

$$C(\omega,\zeta) = \frac{S(\omega)}{2\pi B} \sum_{m=1}^{M} b_m e^{-jkr\cos(\varphi-\theta_m)} \qquad \text{B.9}$$